TAMPERE UNIVERSITY OF TECHNOLOGY
Degree Programme in Information Technology

VALTTERI SAARI

ANALYSIS OF STRAIN IN HIGH STRAIN RATE COMPRESSION OF WOOD USING AN IMAGE BASED ANALYSIS METHOD

Master of Science Thesis

Examiners: Prof. Ari Visa
Pentti Saarenrinne, Tomas Björkqvist
Examiner and topic approved in the Information Technology Department Council meeting on 14 January 2009

Abstract

TAMPERE UNIVERSITY OF TECHNOLOGY
Master's Degree Programme in Information Technology
SAARI, VALTTERI: Analysis of strain levels in high strain rate compression of wood using an image based analysis method
Master of Science Thesis, 67 pages, 6 Appendix pages
April 2009
Major: Signal Processing
Examiners: Professor Ari Visa, Pentti Saarenrinne, Tomas Björkqvist
Keywords: high strain rate compression, local strain, high speed image acquisition, correlation analysis

Properties of wood samples in the mechanical pulping process can be studied using high strain rate loading tests. The mechanical properties are usually measured as a stress-strain relation. However, wood has an inhomogeneous structure and its properties are greatly affected by environmental factors. Because of the inhomogeneous structure of wood, the average strain over a large sample having several annual rings is not a satisfactory measurement. The local strain levels in the wood need to be defined. This thesis presents a measurement technique based on high speed image acquisition and correlation-based image analysis that allows the definition of the local strain levels in the sample during deformation. The main goal of the work was the implementation of a high speed image acquisition system and analysis algorithm as well as to complete the measurements. A representative number of samples are analysed to ensure the efficacy of the method and certain conclusions can be drawn concerning the behaviour of the wood.

The thesis consists of three parts. The first part presents the measurements along with the test samples and the testing device. The high speed camera and camera optics that were used are also described. The choice of illumination method is discussed and finally there is an account of problems faced during the measurements. The second part of the thesis considers the image analysis algorithms. There is also a brief consideration of several alternative methods followed by an explanation of the basic principles of the Digital Image Correlation (DIC) algorithm. The second part concludes with an explanation of the algorithm used, which employs the same principles as DIC. The final section presents the calculated strain levels from the chosen samples.

The high speed recording of the high strain rate loading process worked well and almost all the test cases were successfully recorded. The analysis of the test cases yielded positive results. The strain in the sample focussed on a few narrow regions. The wood in these regions underwent high deformation the while rest of the sample remained unaffected. In addition the fatigue level of the samples and test temperature was observed to have an effect on the strain levels in the sample.

Tiivistelmä

TAMPEREEN TEKNILLINEN YLIOPISTO
Tietotekniikan koulutusohjelma
SAARI, VALTTERI: Paikallisten myötymien määrittäminen nopeassa puunpuristuksessa käyttäen kuva-analyysiin perustuvaa mittausmenetelmää
Diplomityö, 67 sivua, 6 Liitesivua
Huhtikuu 2009
Pääaine: Signaalin Käsittely
Tarkastajat: professori Ari Visa, Pentti Saarenrinne, Tomas Björkqvist
Avainsanat: nopea puunpuristus, paikallinen myötymä, suurnopeuskuvaus, korrelaatio analyysi

Puun käyttäytymistä mekaanisen massan valmistuksen aikana voidaan tutkia nopeilla puunpuristustesteillä. Kuormituskokeessa puunäytteeseen kohdistetaan voima, jonka vaikutuksia mitataan muodonmuutoksena näytteessä. Koska puun rakenne on epähomogeeninen, ei keskimääräinen myötymä ole riittävä mitta muodonmuutokselle, vaan tarvitaan tietoa paikallisista muodonmuutoksista. Tässä työssä esitellään mittaustapa, jossa käytetään suurnopeuskuvausta ja digitaalista kuvankäsittelyä määrittelemään paikalliset myötymät testinäytteissä.

Työ koostuu kolmesta osasta. Ensimmäinen osa on mittaukset. Tässä osassa esitellään näytteet, suurnopeuspuristuslaite sekä suurnopeuskuvauslaitteet. Toinen osa käsittelee kuvankäsittelyä. Siinä esitellään työtä varten suunniteltuja algoritmeja, kirjallisuudessa esitettyjä algoritmeja sekä tässä työssä käytetty algoritmi. Viimeisessä osassa on laskettu paikallisia myötymiä valituille testinäytteille.

Mittausmenetelmä toimi suunnitellusti ja suurnopeuskuvaukset saatiin suoritettua lähes kaikille testinäytteille. Lopputulokseksi lasketut myötymät osoittivat, että puun muodonmuutoksessa on suuria paikallisia eroja. Osa-alueet näytteissä pysyivät lähes muuttumattomina, kun taas toisissa osissa puu menetti yli puolet alkuperäisestä pituudestaan. Alueet, joissa oli eritasoiset muodonmuutokset, näyttivät sijoittuvan eri kohtiin puun vuosirenkaita.

Preface

This work carried out as part of the Nordic Energy Research funded project, Basic Phenomena in Mechanical Pulping. UPM-Kymmene Oyj, Stora Enso Oyj, Metsäliitto Group and Myllykoski Corporation were the other main sources of funding for this work. The goal of the project is to gain fundamental information on the behaviour of wood and fibres in the mechanical pulping process and use this information to reduce the level energy consumption in the process. The project is undertaken in co-operation with KCL, TUT (Tampere University of Technology), HUT (Helsinki University of Technology), Mid Sweden University and Norwegian Technical University.

I was introduced to the topic by Tomas Björkqvist, who is the project's contact person in TUT. I would like to thank Tomas for suggesting this interesting subject and for his invaluable help during the measurement trip. I also wish to thank my examiner, Ari Visa, for his help and advice during this Master's thesis. I gratefully acknowledge the support of my supervisor, Pentti Saarenrinne, throughout this study, especially for his help with the high-speed cameras and lasers. I also wish to thank Alan Thompson for proofreading. My thanks go to all the people in the department, KCL and in Sweden who helped during the measurements.

Special thanks are due to Antero Saari for his kind offers of help.

Finally, special thanks to Ilta Saari for helping me to take my mind off the work once in a while.

I needed it.

Tampere 11.3.2010

_____

VALTTERI SAARI

Valtteri.Saari@tut.fi

Table of contents

Abbreviations

ε	strain
σ	stress
AD	analog to digital convertion
Arg:Ion	argon ion laser
CCD	Charge-Coupled Device
CMOS	Complementary Metal Oxide Semiconductor
DIC	Digital Image Correlation
DSDM	Digital Speckle Displacement Measurement
ESP	Electronic Speckle Photography
FFT	Fast Fourier Transform
fps	frames per second
Nd:YLF	Neodymium: Yttrium Lithium Fluoride laser
PIV	Particle Image Velocimetry
RMS	Root Mean Square
spf	seconds per frame
TTL	transistor-transistor logic

1 Introduction

This work forms part of a project studying basic phenomena in mechanical pulping. Pulping is a process where fibers are separated from the wood used in papermaking. The pulping process can be either mechanical or chemical. Compared to chemical pulping mechanical pulping uses wood more efficiently, but also consumes more energy. There are several mechanical pulping methods. Traditionally the mechanical pulp process involves grinding small wood logs with grindstones. Instead of grindstones many modern mills use refiner plates into which the wood is fed in the form of small chips.

This study investigates the high strain rate compression of the wood. The aim was to study the behavior of the wood under conditions resembling those of mechanical pulping processes. The tests were performed in a split Hopkinson pressure bar which can generate similar strain rates to those in the mechanical pulping process. The compression of the wood samples in the split Hopkinson pressure bar were recorded using a high speed camera. The deformation of the wood was then studied by analyzing the recorded image sets using a correlation-based image analysis algorithm. The aim of the analysis was to compute the strain level distributions in the sample so that the local strain levels in different parts of the growth rings can be compared.

Image-based deformation analysis has been used since the camera technology was sufficiently developed. This kind of analysis allows very accurate and flexible measurements and also allows researchers to see what actually happens in materials during loading. The potential applications for image-based analysis methods have always been limited by the camera, laser technology and analysis methods. The rapid development of these areas in recent years has opened up opportunities for the application of image-based analysis methods.

The image analysis algorithms are being constantly developed to keep pace with new applications. The algorithms are based on computing local displacement vectors. The modifications to the algorithms are aimed at improving their accuracy and computational efficiency. One of the first algorithms used in the correlation based strain analysis was digital image correlation (DIC) presented by Sutton and co-workers in their article "Determination of Displacement Using an Improved Digital Correlation Method" which was published in 1983. The DIC algorithm still remains the basis for new algorithms.

The structure of the thesis follows the sequence of the work. Chapter 2 presents the background information to the study and also the basics concerning the deformation of wood. Since strain is the variable to be measured, it is defined along with an introduction to normal strain measuring methods. Next, the structure of wood is

discussed since this has a major impact on its strength. The effects of temperature and moisture on the strength of the wood are then considered. Towards the end of the Chapter there is an overview of how deformation in the wood occurs and finally the results from other studies on the subject are briefly presented.

Chapters 3 and 4 contain the experimental measurements. The samples used in the work are discussed in the Chapter 3. In Chapter 4 the measurement devices and processes are described. The Chapter starts with a description of the split Hopkinson device that was used for high strain rate loading of the samples. The goals for measurements are then presented. The high speed camera used in the recording is described briefly. Next, the choice of the illumination method is discussed. Finally the actual measurement set up and the problems faced during the measurements are described.

The image analysis algorithms are described in the Chapter 5. At first, several analysis methods were considered. These methods could be used in cases where a high enough recording rate could not be attained during image acquisition. The correlation-based analysis algorithms were introduced. The DIC is described in more detail than other algorithms as it is the best known of them and most of the other algorithms follow the same principles as DIC. Finally the algorithm used in this work is described.

Chapters 6 and 7 cover the results and conclusions of the work. First of all the complete strain distributions are presented for each of the eight chosen test samples. Then a comparison, based on the results, is made between to strain in earlywood and latewood. Finally the conclusion and future adjustment are described.

2 High strain rate deformation of wood

The strength of the materials is studied by applying a load to them. The loading creates forces that will cause changes in the shape of the sample. These changes in the shape are called deformations. The strength of the materials can be studied by measuring the deformation that is caused by an external force. The magnitude of the deformation is referred to as the strain. In high strain rate testing the load is applied instantaneously.

When the deformation of wood is studied, the effects of the structure of the wood and environmental effects must be taken into account. Wood has a complex inhomogeneous structure, which causes a variation of the local strain levels inside the wood. Because of the structure of wood, the direction of the loading also has an effect on the strength of the wood. In addition to this the strength of the wood is also affected by the moisture content and is thus subject to the environmental effects. In particular a high moisture content and a high temperature both lower the strength of the wood. All these factors must be taken into the account when the loading of wood is tested.

2.1 Definition of the measures in deformation

Stress and strain are important factors when the deformation of the materials is studied. Definitions of stress and strain and the notation used can be found in the book by R. Hertzberg [1]. Both stress and strain describe the internal forces and their effects inside the material. Stress (engineering stress) σ is defined in *equation*

$$\sigma = \frac{F}{A}, \tag{1}$$

where the F is the force affecting the specimen and A is cross sectional area of the specimen. The unit of the stress is the Pascal (Pa). The same unit is also used for the pressure. Stress is a measure of intensity of the internal reactive forces in a specimen caused by an external force [2].

Strain is used to describe the deformation in the specimen caused by stress. The total strain in the sample can be calculated by measuring the change in length of the sample. Local strain, inside the sample, can be calculated using several measurement points in the sample and calculating distance changes between each of them.

The strain is usually expressed as a decimal fraction or percentage of the total sample length. This expression is called the engineering strain and is definition normally used in the literature. Sometimes engineering strain is also called relative strain or Cauchy strain. The engineering strain ε is defined as change in the length divided by the original length of the specimen. This is shown in the equation

$$\varepsilon = \frac{\delta l}{l_0}, \tag{2}$$

where the l_0 is the original length of the specimen and δl is the change in length during the deformation [1]. Figure 2.1 shows the change in the length of the specimen.

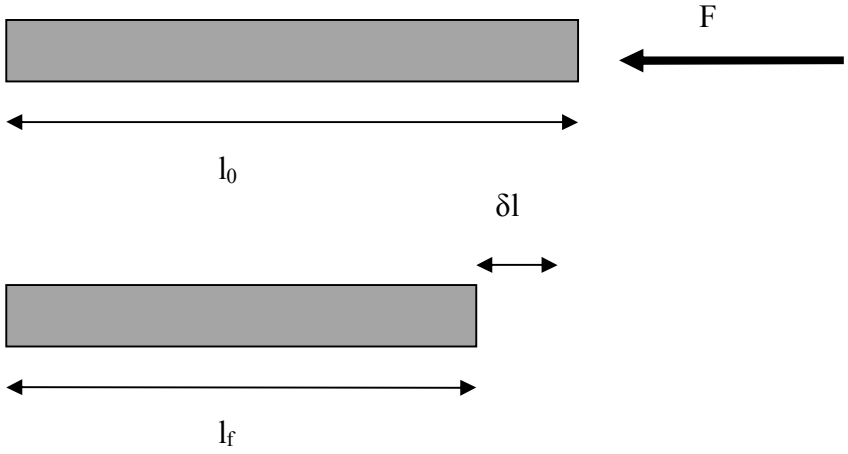

Figure 2.1 Deformation caused by compressive force

From the *equation 2*, it can be seen that engineering strain is a plain, dimensionless number. Sometimes in the literature unit such as mm/mm or µm/µm are used, as a reminder that strain is the change in length. If the strain is negative then the length of the specimen has decreased and the strain is said to be a compressive strain. If the strain is positive then the length of the specimen has increased and the strain is said to be a tensile. Stress can also be shearing. Shear stress causes a change in the orientation of the specimen. The strain caused by shear stress is measured as an angular rotation in radians.

The strain can be defined using the original length and the current length of the specimen. This strain is called the true strain and sometimes it is also called logarithmic strain or natural strain. True strain is defined as the sum of all instantaneous engineering strain levels and it is dependent on the final length of the specimen. True strain ε_t is defined by *equation*

$$\varepsilon_t = \ln \frac{l_f}{l_0}, \tag{3}$$

where l_f is the final length of the specimen and l_0 is the original length of the specimen. In small deformations true strain and engineering strain are practically indistinguishable as can be seen from Figure 2.2. As the level of deformation increases the difference between the engineering strain and the true strain increases and a decision must be made as to which better suits for a particular application.

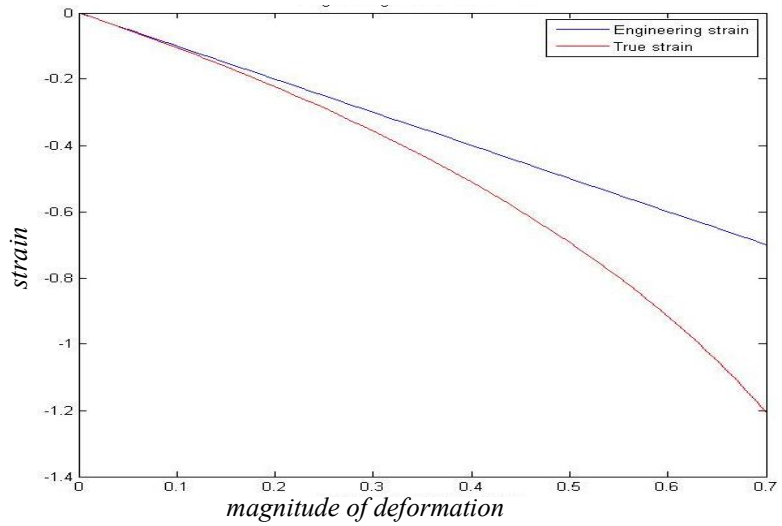

Figure 2.2 Curves showing the difference between engineering strain (blue) and true strain (red) at high deformations.

In cases where there are several different deformations within the same specimen and the strain is calculated in a number of parts, one must remember that the total engineering strain and the sum of engineering strain components may be different. If the sample has two deformations and the first deformation causes change δl_1 in the length of the specimen and the second deformation causes additional change δl_2 to the length of the specimen, then the total engineering strain ε_T as a result of both deformations can be defined by the equation

$$\varepsilon_T = \frac{\delta l_1 + \delta l_2}{l_0}. \tag{4}$$

The sum of the strain levels ε_S is defined by the equation

$$\varepsilon_S = \frac{\delta l_1}{l_0} + \frac{\delta l_2}{l_0 + \delta l_1}. \tag{5}$$

The difference between the total strain ε_T and sum of strain levels ε_S is caused by the change in the length of the specimen during the first deformation. At the beginning of the second deformation the length of the specimen used in the equations has different value depending on which equation is used. This is a typical problem when deformation in specimen is large or takes place in several phases. This problem only applies when the engineering strain is used. In such applications the true strain is the preferred choice as it allows the summation of the strain levels. As long as the original length of the specimen is significantly greater than the change in the length, it can be assumed that the total engineering strain is approximately same as the sum of engineering strain components.

The strain rate is a measure that is used to define the speed and the scale of the deformation process. It is defined as the change of strain with time. A high strain rate means that large deformations takes place during a short period of time and conversely a low strain rate means that a small deformation takes place over longer period of time. Because the strain itself has no unit the unit for the strain rate is s^{-1}. In material testing the strain rate is an important measure, because materials behave differently at different strain rates.

The properties of the materials can be presented with their stress-strain diagram. The stress-strain diagram shows the relation of simultaneous values of a stress and strain [2]. The strain is in the x-axis and the stress is in the y-axis. The curve shows the amount of stress needed for certain strain level. The deformation in the sample normally causes changes in the cross sectional area of the sample, which will affect to the stress.

2.2 Strain measuring

In theory, the strain in a sample is easy to measure. The only parameter that needs to be measured is the length of the sample before and after the deformation. In practice, however, strain measuring is not that straightforward. Usually in practical applications continuous strain measurements are needed. Typically the measuring device needs to be attached to sample so the deformation can be measured throughout the process. Attachment of the measurement devices is crucial thing as it may not have an effect on the deformation and it must transmit the deformation to a device which records the signal. One way of avoiding attachment of a device is to use an optical measurement system, thus the measurements can be made from a distance without disturbing the deformation. An optical measurement system can be, for example, a video camera.

One thing to note in strain measurements is that the strain is always an average strain over the measured length. Also the change in the length only defines the strain in that direction. This is acceptable in many experiments especially if the test sample is of material that has a homogeneous structure and the external forces are applied uniaxially. In that case it can also be assumed that all the strain in the sample is distributed homogeneously. In the case of materials with an inhomogeneous structure the deformation will not be homogeneous. The strain will vary locally. Several measurements are needed to compute the local strain in such a sample. The overall strain can be calculated by combining all the local strain measurements. This can be undertaken by using several measurement devices on the same sample or more conveniently by recording the deformation as digital images and using image analysis techniques to calculate the local strain at particular points.

Traditional strain measuring devices include extensometers and strain gages. They are cheap and easy to use and work well in many applications. However in scientific research their limited ability to model complex deformation is a severe downside. For that reason in scientific research strain analyses are usually performed with more sophisticated measuring methods. Modern image acquisition techniques and digital image analysis are the tools needed for more complex strain analysis. Usually it is useful to combine different measurement devices and techniques so that results from the different techniques can be compared.

Extensometer

An extensometer is an instrument designed for measuring deformation of samples. The device is attached to the specimen at two locations. The change of length in the specimen between these two attachment points is transmitted into the actual measuring device. Several different types of extensometers capable of measurements at different levels of accuracy exist. Optical extensometers use lasers to measure the change of length. [4]

Strain gage

A strain gage is the most common strain measuring device. It is also sometimes called a strain gauge. It was originally invented by Edward E. Simmons and Arthur C. Ruge in 1938. It is electronic device, which measures the change in electrical resistance which varies in proportion to the level of strain so it is actually a kind of extensometer. A strain gage consists of a thin back wall, which is attached to the test specimen. The back wall is called the carrier. In the carrier there is thin wire arranged in a grid pattern parallel to the direction of strain to be measured. The resistance of the wire is measured between the two end nodes. The structure is shown in Figure 2.3

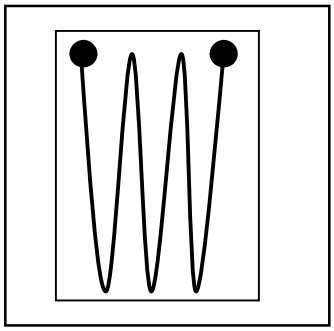

Figure 2.3 The structure of a strain gage

When the sample is deformed, the carrier transfers that deformation to the wire grid and that will cause a change in the length and thickness of the wire. These changes cause a change in the resistance of gage. If the wire becomes shorter and thicker the resistance will decrease but if the wire becomes longer and thinner the resistance will increase. This change in resistance is easy to measure and from that change the strain can be computed. In large applications the strain can be measured by combining the simultaneous measurements from several strain gages or from several different measurement devices. [5, 6]

Image based analysis methods

Image based strain analysis methods have gained popularity in scientific research due to their flexibility and accuracy. In these methods the deformation of the specimen is recorded as a series of images. The strains can be extracted from these images using image analysis algorithms. These methods hold many advantages over the more traditional strain measuring methods. Images can be recorded from a distance and so the recording does not affect the deformation and the resulting strain measurements that are computed. With modern high-speed cameras and pulse lasers a series of images can be recorded throughout the deformation, so even fast and complex deformations can be accurately quantified. One must remember that the test specimen must have some distinguishable pattern on its surface so that differences between images can be detected. If the specimen itself does not have a suitable surface, this can be added by, for example, using spray paint.

Several different algorithms exist for analyzing a deformation process that is recorded as series of images and most of these algorithms are based on the same principles. The best known method is digital image correlation (DIC) first suggested by Sutton and co-workers [7, 8, 9]. Another approach called digital speckle displacement measurement (DSDM) was suggested by Chen and co-workers [10, 11, 12]. Electronic speckle photography (ESP) was suggested by Sjödahl and Benchert [13, 14,15]. Particle image velocimetry (PIV) that is used in fluid dynamic research uses the same principle. The basic idea behind these algorithms is to identify local displacements and combine them to produce a complete map of the deformations or movements.

2.3 Strain in wood

Wood is a challenging subject for strain analysis because of its inhomogeneous structure and its dependence on environmental factors. The inhomogeneous structure causes variations in the strength of the wood depending on the direction of the loading. Also the deformations inside the wood will depend on the location. The main environmental factors which affect the strength of wood are temperature and moisture content.

2.3.1 General structure of softwoods

Generally, wood is divided in to softwood and hardwood. Softwood is produced by conifers (needle-bearing trees) and hardwood is produced by angiosperm trees (broad leaved). The test samples in this work were taken from Norway spruce growing in Finland (Picea abies). This is a softwood, so the general structure of softwoods is described here. The structural differences between softwood and hardwood are at a cellular level.

Wood is an organic material that has a complex structure. The structure is created during the growth process of the tree and all the parts of the structure have specific functions. The best way to understand the structure of the wood is to start with observation of the cross-section of the stem at a macroscopic level and then to move to smaller and smaller structures until finally the cellular structure is observed. Three axes are used to define directions in the wood. Two of the axes represent different growth directions. The different axes are shown in the Figure 2.4. The longitudinal axis is the direction of the stem. The radial direction is the direction from middle of the trunk to outside and the tangential axis is the direction of the tangent of the woods layers.

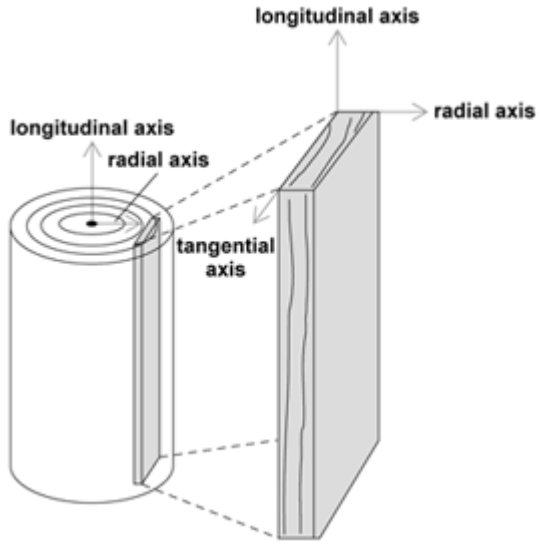

Figure 2.4 Different axes inside wood [16].

The cross-section of the trunk of a tree consists of different layers. Figure 2.5 shows the cross-sectional image of across the trunk. The outermost layer is the bark. Inside the bark is the actual wood section known as xylem. Xylem is divided into the outer part called sapwood and the inner part that is called the heartwood. Sapwood is the part of the tree where living cells are located. After a certain amount of time the cells die and became part of the heartwood. Because the cells in the heartwood are dead they have no other function than to support the tree. The sapwood performs the roles of support, water conduction, and nutrition storage.

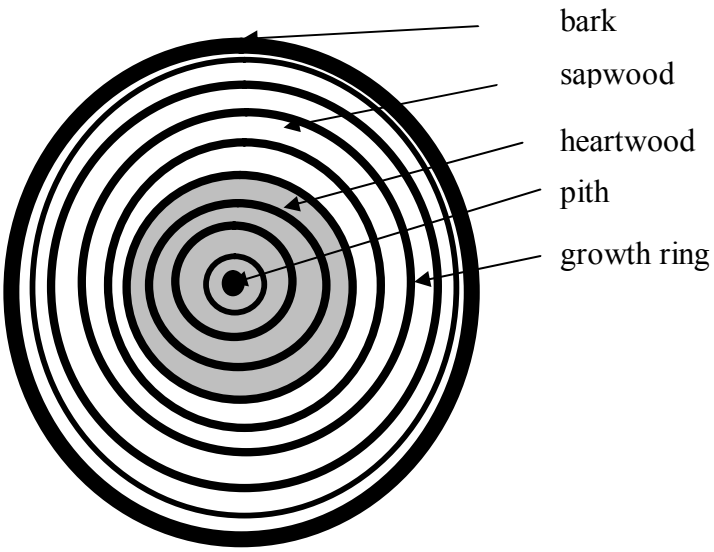

Figure 2.5 Different layers in the cross-section of a tree trunk.

The growth of the tree takes place just under the bark. The bark consists of two layers known as outer bark and phloem (inner bark). The layer between the bark and xylem is called the cambium. Cambium is the part where the growth of the tree takes place in the tangential and radial directions. This growth is called secondary growth. Primary growth takes place at the tip of the branches and the stem and causes longitudinal growth. The cells in the cambium divide creating the phloem cells outwards and xylem cells inwards. The layer of xylem that was created during one growth season is called a growth ring or an annual ring. The thickness and the colour of the growth rings depend on the climate and the growing environment. In addition to growth rings narrow radial stripes can also be seen. These stripes are called rays. [17, 18, 19]

The growth rings consist of two layers – the thicker and lighter earlywood layer and thinner and darker latewood layer. The growth rings of the Norway spruce are shown in Figure 2.6. Different colours of the layers are clearly visible in trees that grew on climate where the growing seasons are separated by winter. The earlywood layer is created at the beginning of the growing season when the growth of the tree is fastest and the cells that are created are large. After some time into the growing season the growth

slows down and the cells that are produced during the rest of the growing season are smaller and have thicker walls. The part of the growth ring that was created at the end of the growing season is the latewood layer. Sometimes the part that has grown between the early- and the latewood is called the transition wood but the division to different zones is not exact. Because of the cell size and the cell wall thickness the latewood layer is harder and denser than the earlywood layer. The transition from the latewood back to earlywood is sharp because the growth stops at winter but begins rapidly again at the new growing season. [17, 18]

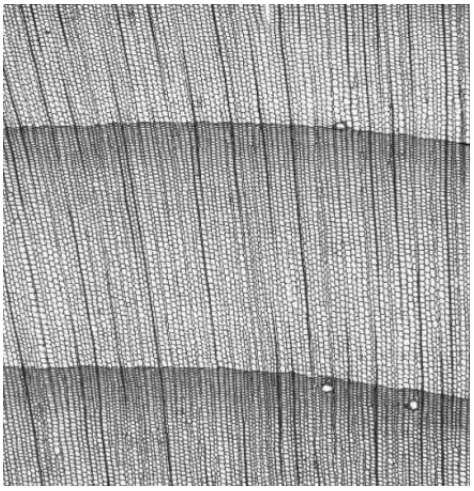

Figure 2.6 Close up view of the growth rings of the softwood [20]

If the stem of the spruce is bent, it will form reaction wood to correct the orientation of the stem. The reaction wood in spruce is harder than other wood. It will form below the bent part to push it up. [17]

The cell structure of the softwood is presented in the Figure 2.7. In softwoods the stem consists of two types of cells. There are long and narrow tracheid cells, which occupy 95% of the volume of the stem. They are 2-4 mm in length with a thickness of around 20-40 µm. Due to their shape the tracheid cells are called fibers. Tracheid cells are located mostly in the longitudinal direction of the stem. They are hollow so they are used for the transportation of water and as storage. The space inside the tracheid is called the lumen. The volume of lumen is dependent on the thickness of the cell wall. In the cell walls there are small holes called pits that connects the cells. Cell walls in the latewood are much thicker than cell walls in early wood. Due to the differences in the diameter, wall thickness and coarseness, earlywood and latewood cells differ considerably in their properties. [17, 18]

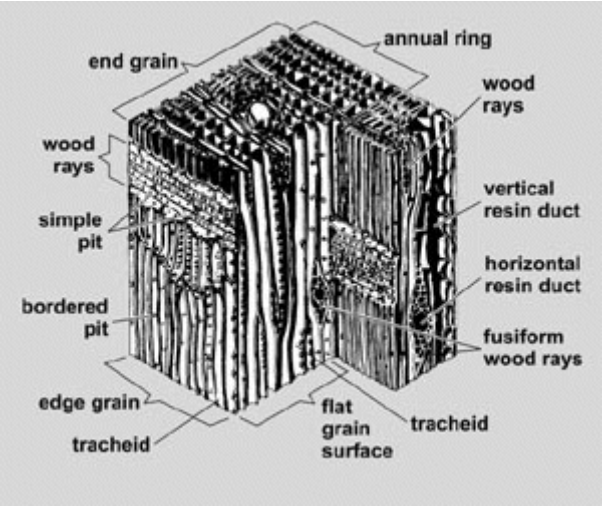

Figure 2.7 Different cell structures in softwood [21]

The other cell type is parenchyma cell. Parenchyma cells are shorter than tracheids. Most of the parenchyma cells are located in cell structures known as rays. Rays are located in the radial direction of the stem and they move water and other substances to the cambium. [17]

2.3.2 Effect of the environment on the strength of wood

The environment has a huge effect on the properties of the wood. The two biggest environmental variables are moisture content and temperature. Both the hollow cells and cell walls absorb water easily. The water content has a dramatic effect on the mechanical properties of wood. The increased moisture content will lower the strength of the wood. The temperature will have an effect on the cell walls that consists of polymers such as cellulose, hemicelluloses and lignin. A high temperature will soften the polymers so the strength of the wood will diminish. When the rise in temperature is combined with moisture the softening of the polymers will take place at a lower temperature than when the wood is dry. The temperature required to soften the polymers of dry spruce can be as high as 180 °C whereas the polymers of moist wood are softened in the region of 90 °C. [16, 18]

Although the general effect of moisture and temperature on wood is known there is still much to learn about their combined effect. One of the interesting questions is whether the temperature and moisture will have the same effect on the earlywood and latewood or are some layers affected more severely. Because of the inhomogeneous structure of the wood it is to be expected that there will be differences in how moisture and temperature affect to the earlywood and the latewood.

2.3.3 Deformations in the structure of wood

Stress causes deformation in the structure of wood. The deformation does not take place homogeneously and the amount of the deformation varies locally. At the cellular level the deformation is seen as a buckling of the cell walls. The deformation of the wood goes through several phases that can be distinguished in the stress-strain behavior of the sample.

Small deformations in the wood are elastic. In elastic deformation the shape and size of the specimen is restored when the force is no longer applied. In wood this means that in a small deformation the cell walls deform elastically. In elastic deformation, stress and strain are directly proportional. Above a certain strain level, which depends on the wood and the environment, the shape of the wood sample does not recover after the forces are removed. This deformation is partially plastic. In plastic deformation the cell walls buckle plastically, meaning that the cell walls are damaged and they will not recover their original shape completely. The third phase in the deformation of wood is densification. This happens when the cell walls start to touch each other. [16, 22]

Other deformation types are fatigue and fracture. Fatigue results in a very small structural defect that is caused by repeated deformation. Even though the shape of the wood is reversed in elastic deformation, each deformation will cause faults in the cell walls at a molecular level. These faults will accumulate and change the strength of the wood. Fracture of the material is caused when the forces causing the deformation exceed the local strength. At that point a crack starts to appear and stress relaxation tarts near the crack.

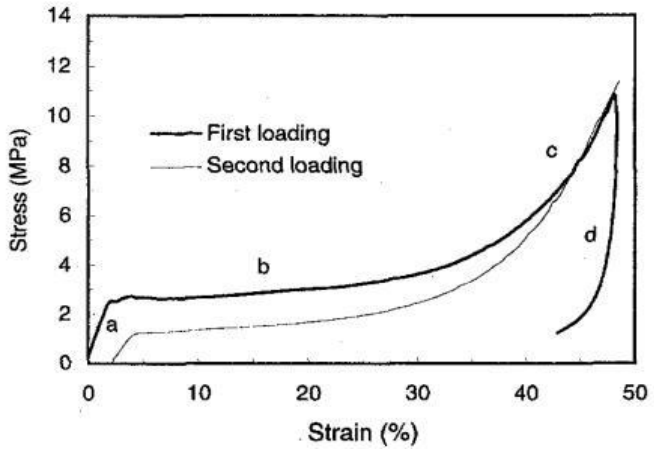

Figure 2.8 Stress-strain diagram of Norway spruce. (a) elastic deformation (b) plastic deformation (c) densification (d) return of the shape after the load is removed [22]

The different deformations can be observed from the stress-strain curve of the wood in Figure 2.8. The beginning of the curve is usually steep and a lot of stress is needed to increase the strain. This part of the deformation is the elastic deformation and for wood it lasts only a little while. Because the stress and the strain are directly proportional in

elastic deformation this part of the curve is a straight line. The steep beginning of the curve is followed by the long plateau where the stress does not increase much even though the strain is increasing. This part of the curve corresponds to the plastic deformation and buckling. At the end of the curve it starts to rise steeply again. The stress increases but the strain remains the same. This part of the curve represents the densification. If the compression is continued the sample will eventually crack. Figure 2.8 also shows that less stress is needed to cause the equivalent amount of strain in a second loading than was needed in the first loading. [22]

2.3.4 Recent studies of high strain rate compression of wood

High strain rate compression of wood can be studied as part of the fundamental research for mechanical pulping. Our project was to research the effect of temperature and fatigue on the local stress-strain behavior of the wood. Several other studies exist in the same area.

Andreas Uhmeir and Lennart Salmén studied the effect of strain rate and temperature on the strength of wood in their article “Influence of Strain Rate and Temperature on the Radial Compression Behavior of Wet Spruce“. In the article they noted that both variables had great effect on the compression. [22]

Svante Widehammar studied the influence of strain rate, and moisture content and the loading direction on compression of spruce in the article “Stress-strain relationships for spruce wood: Influence of strain rate, moisture content and loading direction”. As a result he noted that dry wood has a much higher strength than wet and compression in the longitudinal direction requires much higher stress than in other directions. [23]

3 Test samples

The deformation of wood samples under the conditions found during mechanical pulping is studied in this work. The wood samples were taken from Norway spruce, because it is the most common wood used in mechanical pulping. The goal was to compare the magnitude of the deformation in the early and latewood parts of the growth rings. The test samples were provided by KCL. Before the measurements part of the samples was fatigued. The intention was to keep the moisture content of the samples the same as the moisture content of fresh wood. Before the measurements were made the surface of the samples was painted so as to give better surface images for analysis.

3.1 Properties of samples

The wood in the measurements was taken of fresh Norway spruce. The samples were cut into cubes with a thickness of 6 mm and length and height 12 mm. The loading of the samples would be aimed at the largest side so the compression would take place in the radial direction. The growth rings would visible at the front side of the samples. Typically there would be two or three growth rings in the each sample as can be seen in Figure 3.1. The growth rings were usually in a vertical direction but there were some variations in orientation between samples. A series of samples can be seen on the left of Figure 3.1.

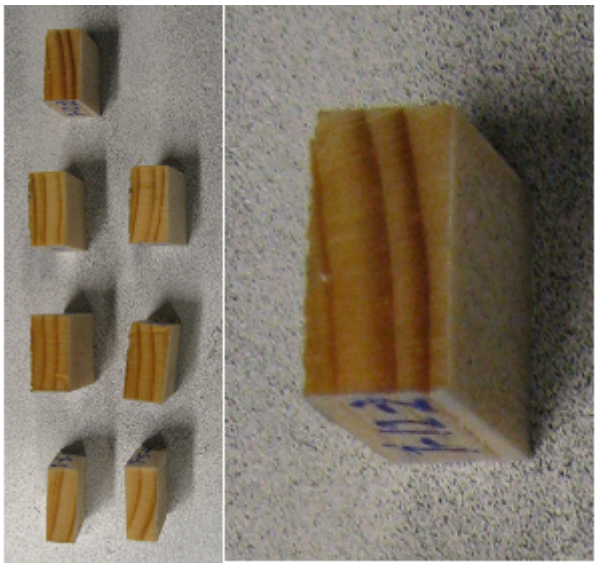

Figure 3.1 Series of test samples to be loaded at 130 °C. On the right is close up image of one of the samples

Most of the samples were fatigued before the measurements. This was done to determine the effect of the fatigue level on the strength properties of the different parts of the wood. The fatiguing does not change the dimensions of the wood, but it does destroy or modify the cell structures thus affecting the strength of the wood. The wood was fatigued using the KCL modulated loading device which applies compressive pulses at a frequency of 500 Hz with an amplitude of about 1 mm. The samples were divided into different groups depending on the fatigue level of the wood. The fatigue level was defined according the number of pulses used when the fatiguing was applied. The fatigue levels used were 6,000, 12,000 and 20,000 pulses. There were also reference samples that were not fatigued at all. The samples were labeled to keep track of the fatigue level of the samples. In Figure 3.1 the label can be seen at the bottom of the sample in the close up image of the sample.

Table 3.1 Sample labels and testing conditions

Sample name	File name	Test date	Test time	Temperature [C]	Thickness before [mm]	Thickness after [mm]	Weight before ESHD [g]	Weight after ESHD [g]
B-1-4-7 : 20k	011	2.12.	14:50	20.0	6.26	6.00	0.5652	0.5518
B-1-4-3 : 20k	010	2.12.	14:44	20.0	6.20	6.10	0.5815	0.5727
B-1-12-6 : 0k	013	2.12.	15:10	20.0	6.31	6.18	0.5032	0.4968
B-1-12-3 : 0k	012	2.12.	14:59	20.0	6.18	6.13	0.6052	0.5927
B-1-11-5 : 6k	014	2.12.	15:55	20.0	6.19	6.09	0.4460	0.4342
B-1-11-7 : 6k	017	2.12.	16:12	20.0	6.23	6.13	0.4568	0.4503
A-1-20-2 : 12k	016	2.12.	16:07	20.0	6.19	6.13	0.5744	0.5640
A-1-20-5 : 12k	015	2.12.	16:01	20.0	6.21	6.05	0.5338	0.5283
A-1-24-6 : 0k	009	2.12.	14:37	20.0	6.16	6.08	0.6305	0.6112

In Table 3.1 the labels for first series of test samples are given in the column “Sample name”. After the sample name is the fatigue level of the sample. Other columns in the table give the measurement time and conditions and weight and thickness before and after the testing. The table was completed during the measurements. The tables that show the labels for all the test samples are included in the appendices.

3.2 Pre-treatment of the samples

The moisture content of the fresh wood is approximately 45% and the aim was to keep all the samples at that moisture content until the measurements were complete. Because of the long that it took before the measurements could be started, the samples had lost some moisture although they were preserved as well as possible. At one point the samples were remoistened. Remoisening of the samples was a long process because the moisture must be distributed evenly within the sample. The moisture content was measured using the weight of the sample as an indicator. In the end most of the samples had an acceptable moisture content although there was no exact indication that the moisture was evenly distributed within a sample.

The front face of the samples was smoothed by cutting away a small slice of wood with a microtome. A microtome is instrument normally used to take thin and transparent slides from organic samples to be analyzed in a microscope but in this case it was used to smooth the surface of the sample. The surfaces of the samples were smoothed to improve the accuracy of split Hopkinson measurement and to get a better surface for painting and to detect the growth rings more clearly.

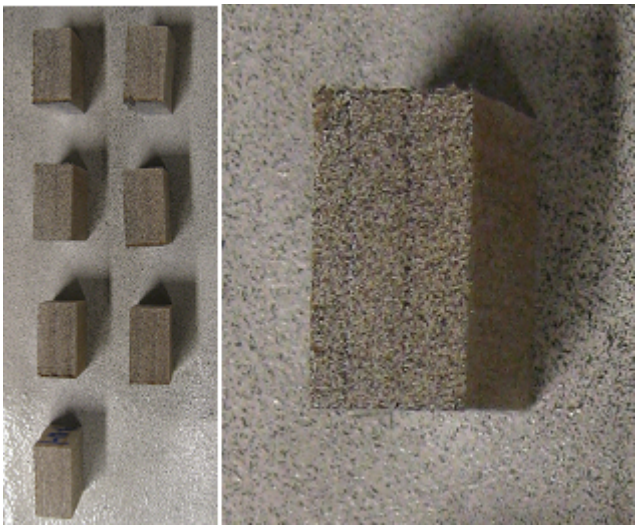

Figure 3.2 Images of test samples after the painting process.

Samples were painted with white and black spray paint. The painting was done to create a random surface pattern that could be tracked with image analysis algorithms. First a thin layer of white paint was sprayed onto the sample. The white color will increase the brightness of images and give high contrast with black paint so the surface pattern would have maximum contrast. The downside of spraying with a layer of white paint is that the growth rings are harder to detect. A light spray of black paint is sprayed on top of the white layer. A series of painted samples can be seen on the Figure 3.2. Good way is to spray upwards so the paint will drop from the samples. When the paint was sprayed in this way the speckles were round and distributed randomly.

The final procedure applied to samples before measurement was to weigh them and to measure their thickness. The moisture content of the samples was monitored by observing the weight of the samples. This final measurement was carried out to confirm the moisture content of the samples.

4 Measurements

In this work the measurements consisted of high speed recording of the high strain rate compression of the wood samples in the split Hopkinson device. Because the analysis would be based on these images the image acquisition was the most important part of the work. If the image acquisition yields high quality image sets, the analysis of the images would be easier and the measurements would yield more accurate and reliable results. If the images are of low quality a lot of effort must be used just to get reliable results or new images must be acquired. In this work the image acquisition was undertaken in challenging conditions and there was no possibility of acquiring new images. The image acquisition procedure was very carefully planned and a lot of testing was undertaken in advance to find the right equipment.

The measurements were undertaken during one week using split Hopkinson pressure bar at the Mid Sweden University at Sundsvall. The measurements were part of a larger project, where similar samples were compressed and studied differently. The high-speed recording was added to the final measurements of the project so there was no chance of doing new recordings if image acquisition had failed. For that reason a lot of testing was undertaken in the laboratory of the Department of the Energy and Processing engineering, where a set up was built to replicate the conditions at shooting location. The testing was undertaken to exclude all the possible problems that could occur in the final measurements.

4.1 Split Hopkinson pressure bar

The measurements were undertaken in the split Hopkinson pressure bar at the Mid Sweden University. The split Hopkinson bar test is the most commonly used method for determining the properties of the materials at high rates of strain [24]. It was originally suggested by Bertram Hopkinson in 1914 as a way to measure stress pulse propagation in a metal bar and the method was later refined by R.M. Davies and H. Kolsky to measure stress and strain by using two Hopkinson bars in series [25]. Since then the method and device have remained practically unchanged.

The structure of split Hopkinson bar can be seen on the Figure 4.1. The device consists of two long symmetrical metal bars. The bars are called the incident bar and the receiver bar and they are located horizontally along the same axis. They are allowed to move freely in the direction of the axis. The bars are typically made of a high-strength metal, such as steel [26]. However, a softer material is needed for bars when the material to be tested is also soft. Generally the bars need to be of material with known properties and the stiffness properties of the material should be as close to the properties of the test material as possible.

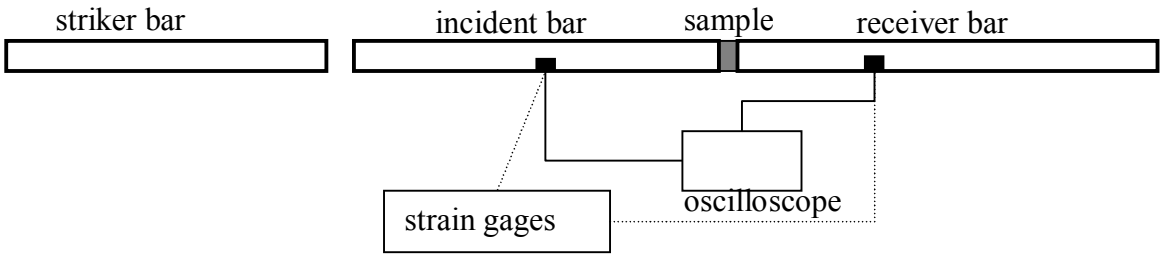

Figure 4.1 Structure of split Hopkinson pressure bar.

In the test the specimen is sandwiched between the bars. At the open end of the incident bar is gas gun, which is used to shoot the projectile at the end of the incident bar to start the compression. The projectile is called the striker bar. By varying the pressure which is used to shoot the striker bar different strain rates can be generated by the device. The strain rates generated by split Hopkinson bar are usually form 200 s^{-1} to 1,000 s^{-1} [26].

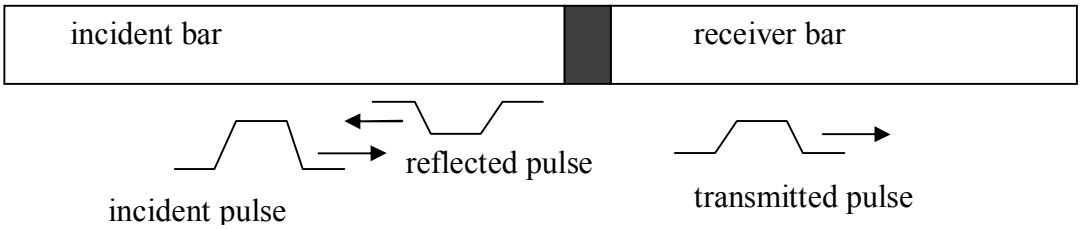

Figure 4.2 Movement of elastic pulses inside the metal bars at split Hopkinson device

The basic functional diagram of the split Hopkinson device is shown in Figure 4.2. When the striker bar hits to the incident bar, an elastic pulse is generated inside the incident bar. This pulse is called the incident pulse. This incident pulse will traverse through the bar towards the test specimen. At the interface of the bar and the specimen a proportion of the pulse is reflected back while part of the pulse will be transmitted into the specimen. Then the pulse will traverse through the specimen and at the interface between the specimen and the receiver bar, part of the pulse is reflected back while part of the pulse will travel on to the receiver bar. Inside the incident bar reflected pulse will reflect back again from the open end of the bar and will hit the specimen again.

The proportion of the pulse that will be reflected back at the interface of the bar and the specimen is dependent of the properties of the material of the bars and the specimen. If the bar is much harder than the specimen a large portion of the pulse will reflect back and only very small proportion will go to the specimen. The reflection of the elastic pulse in the incident bar causes several compressions in the specimen with one striker bar hit. Normally the measurements are concentrated on the first compression.

The strain is measured in a split Hopkinson device by using strain gages attached to the incident and receiver bars. Strain gages signals are received from both bars. These signals measure the elastic pulses in the bars. From the strain gage in the incident bar both the original pulse and the reflected pulse are detected and from the receiver bar the transmitted pulse is measured. The stress-strain curve for a sample can be computed from these three pulses. A complete description of the stress-strain analysis at Mid Sweden University is given in “A method for dispersive split Hopkinson pressure bar analysis applied to high strain rate testing of spruce wood” by S. Widehammar [27].[24, 26]

The split Hopkinson bar used in this work was modified version of split Hopkinson device. The difference was that the whole device is encapsulated within a pressure vessel. The encapsulation can be seen in the Figure 4.3. Bars and the test sample are located inside the vessel. This modification allows the user to control the temperature and the pressure during the tests. The ability to control the environment is important when the properties of test material are greatly affected by the environment, which is the case with wood. The temperature and the pressure are controlled by hot air and steam.

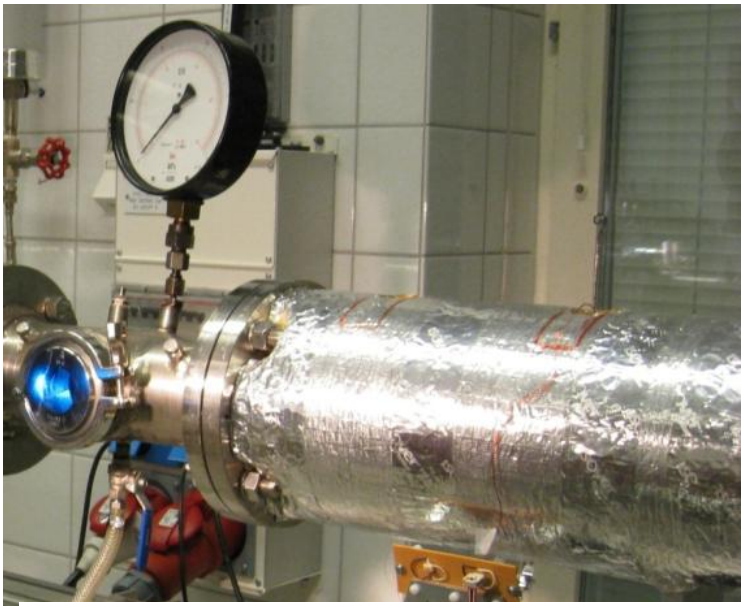

Another adjustment that was made to the device was making the incident bar and the receiver bar of special aluminum instead of the more common steel. The aluminum bars suit the testing of wood samples as they are softer than steel bars. By using softer bars a better signal is received from the strain gage transducer in the receiver bar.

Figure 4.3 Encapsulation of split Hopkinson bar

Because of the encapsulation of the split Hopkinson device the view of the sample was limited. There was only a small circular window with a diameter of 40 mm in the front face of the device. Recording and illumination of the process is performed through this window.

4.2 Process to be recorded

The process to be recorded was a high strain rate compression of the moist wood samples at different temperatures in the encapsulated split Hopkinson device. The temperatures that were used in measurements were 20 °C, 65 °C, 105 °C and 130 °C. At each temperature a series of numbered samples were be tested. The process was started by clamping the sample between incident and receiver bars. The samples were placed so that the growth rings faced the front and the loading would take place along the radial axis. The face of the sample that was visible was 10 mm in height and approximately 6 mm in width. The visible face of the sample was painted with white and black spray paint so as to have a random speckle pattern on the surface. The incident bar would then be gently loaded so as to keep the sample tightly between the bars. When the sample was in place, the device door was closed and the temperature inside the device was raised to the test conditions.

The temperatures used were chosen taking into account the properties of the split Hopkinson device and the wood. Room temperature was used as a reference point. A temperature of 65 °C can be attained at normal air pressure. The temperatures were chosen to be in the range where the fibers in the wood starts to soften. To attain the two highest temperatures the pressure inside the device was also raised.

The measurement process was started by launching the striker bar with a gas gun. The pressure used to launch the striker bar was kept constant. When the striker bar hits the incident bar it causes a compressive pulse inside the incident bar. The pulse will reflect back from the head of the incident bar. At the end adjacent to the sample a small proportion of the pulse will proceed into the sample and through the sample into the receiver bar. The strain gage transducers will detect the passing pulses. Each pulse hitting the sample will cause deformation of the sample.

4.3 Goals for image acquisition

The aim of the image acquisition system was to receive high quality sets of images that could be used to analyze the local strain levels inside the wood samples. As the main interest was the first compression in the sample, it was essential to get as many frames as possible recorded during that period. At least five or six frames were considered necessary to be able to perform the analyses, but ten frames would be preferable. If it proved possible the later compressions of the sample would also be recorded for possible future analyses. Because the deformation would be analyzed mainly in the direction of the compression, the whole of the sample in the horizontal direction must be included in the frame.

The required recording rate was estimated from earlier high-speed photography tests in a split Hopkinson device. In those tests a recording rate of 20,000 fps was the highest that was used. At that speed approximately five frames could be recorded during the

first compression. It was noted that the signal from the strain gage transducer in the incident bar would last for 200 μs, which would mean that the recording of ten frames would require a recording rate of 50,000 fps. Using this information a recording rate of 20,000 fps was set as a minimum requirement for camera and illumination, but the target was to get equipment with a recording rate as high as possible.

The quality of images is dependent on the resolution and contrast. Both of these properties are to some degree dependant on the recording rate. The resolution required limits the recording rate to be used because high recording rate restrain the attainable image resolution. The main factors affecting the contrast of the image are the focus and the motion blur. Because the surface of the sample is in the same plane all the time, focusing is not a problem even with a small depth of the focus. The image becomes blurred when the exposure time of the recording system is too long compared with the speed of the target and the magnification of the objective lens. The temporal resolution required, which is the inverse of the maximum exposure time, is directly proportional to the speed of the target and inversely proportional to the size of the image area.

4.4 Image acquisition tests

Several tests were performed before the final measurements were undertaken to find the most suitable camera and illumination method that would work under real test conditions in a split Hopkinson bar. A test set up was built in the laboratory of Energy and process engineering at Tampere University of Technology. The set up consisted of a screw vice, which would model the incident and the receiver bar of the split Hopkinson pressure bar, a plywood board with a circular window, which would model the window in the split Hopkinson pressure bar, and high-speed imaging equipment. The set up was built to match the geometry of the actual measurement device (Figure 4.4).

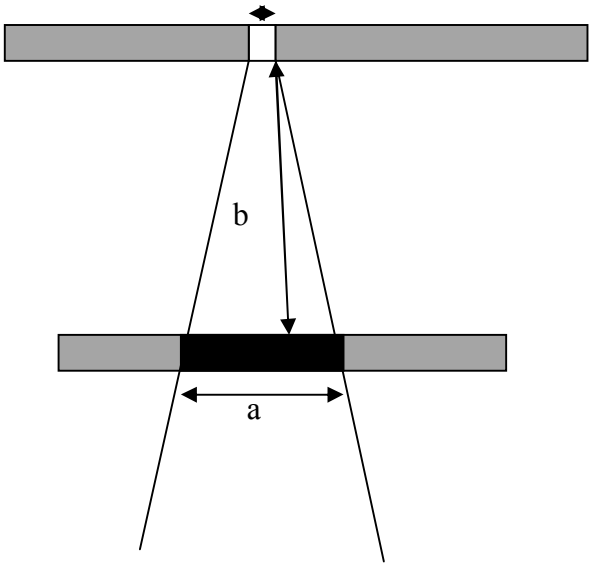

Figure 4.4 Geometry of the split Hopkinson device. a) window diameter 40 mm, b) distance from sample to window 78 mm

Figure 4.5 Testing set up and equipments

A test sample was sandwiched in the screw vice with the jaws of the screw vice representing the bars of the split Hopkinson device. The plywood board was then located in front of the specimen in such a manner that the window was directly in front of the sample at distance of the 78 mm. The diameter of the window was 40 mm. The screw vice and the plywood board were painted with matt black paint to avoid the reflection of the laser light. A picture of the set up is shown in the Figure 4.5. The sample is located at the bright laser spot.

4.5 High-Speed Camera

The high-speed camera that was used in the measurements was a Photron Fastcam SA1.1. The choice of the camera was easy as it is the fastest camera available. It has an image sensor of 1024*1024 pixels and can record full frames with a recording rate of 5400 fps. The maximum recording rate is 675,000 fps. The camera had an internal memory that allowed flexible triggering options as the sequence can be recorded before, after or around the trigger signal. [28]

4.5.1 Camera objective

The camera lens that was used in the measurements was Nikon Teleplus 200 mm. By using a lens with long focal length close up images can be taken of distant objects. In the recording set up all the possible distance was needed as there was not much room for imaging equipment. The angle where the camera and laser could be aimed through the window was narrow. The lens used was the longest that could be obtained and using it gave some extra room for the laser optics.

The downside with the lens with long focal length is that the depth of the field will be narrow. The depth of focus is the range of distance over which the object will appear sharp in the image. That was not a problem in these recordings because at the beginning of the process everything is in the same plane and movement of the plane is minimal. The aperture of the objective was set to be fully open so as to receive as much light as possible. This means that the f-number was set to smallest option available. Small f-number means a reduced depth of the focus, but the brightness of the images was a greater concern than the depth of the focus.

4.5.2 CMOS Image Sensor

The camera used a CMOS image sensor, with a resolution 1024*1024 pixels . There are two types of image sensors mainly used in high-speed cameras - the CCD (Charge-Coupled Device) sensor and the CMOS (Complementary Metal Oxide Semiconductor) sensor.

A sensor consists of discrete pixels and the number of pixels defines the resolution of the captured image. The size of the pixels defines the size of the sensor plate. When light hits the surface of the sensor it causes electrical charges to be generated at each of the pixels. This charge is proportional to the light intensity at that location. The charge at each pixel is first converted to voltage and then to a digital signal.

The difference between the CCD sensor and the CMOS sensor is the time taken to convert charge to voltage. In the CMOS sensor, the charges are converted to voltages at the pixels whereas in the CCD sensor the charges are read from the sensor and then converted. The reading of the voltages from the CMOS sensor is a simpler procedure. The voltages can be made to move to the next pixel in one direction. The outermost voltages are moved into the register in which the voltages are moved one at time to the output node. The reading of the charges from the CCD sensor is done in the same manner. The conversion to voltages is done after the output.

This kind of light sensor can be used at an increased recording rate by using only a proportion of the pixels to capture the light. If only the top half of the pixels are used in image capture, the new image can be taken when the charges or voltages from the first image are moved into the bottom half of the sensor. This allows double the recording rate as when recording the images with full resolution. In the camera used the area of active pixels could be freely chosen.

Because in a CMOS sensor the voltages are generated at the pixels, it is possible to use amplifiers, AD conversion and other operations to the same circuit outside the sensor. Operations can also be added in to the pixels. This will allow CMOS cameras to be faster and smaller than CCD cameras. In a CCD sensor the all of pixels can be used to capture light as there are no additional operations. This allows much more efficient light capture which means that less light is needed to illuminate the target. Another important difference is that because CMOS uses separate charge to voltage converter to each pixel, the output uniformity of the CMOS sensor is lower than that of CCD sensors. The output uniformity is an important factor in determining the image quality. [29]

4.5.3 Automatic triggering of the camera

The camera needs a trigger signal to start recording automatically. Because the camera had an internal memory it could be set in the mode where it continuously records new frames into its memory replacing the oldest ones. In this mode it is possible to define the number of frames that are recorded before the trigger signal. This kind of mode allows very flexible triggering as a full memory of frames corresponds to more than one second of recording. The trigger signal needed could be taken from the strain gage transducer from either of strain gages in the split Hopkinson device. The signal from the incident bar was used. This signal was transformed to a TTL (transistor-transistor logic) signal which was needed for the camera.

4.6 Laser illumination methods

In high speed image acquisition a very powerful light source is needed. The time to illuminate the subject may be only a few microseconds. Lasers allow high energy illumination. With pulsed lasers the light is in short, high energy pulses. A pulsed laser can be synchronised with the camera to provide fast and powerful illumination.

The choice of the illumination method used in testing was not as straight forward as the choice of the camera. The basic requirements for illumination were that it needed to produce sufficient illumination power for recording rates of up to 50,000 fps and it must be suitable to transport to the measurement location. Three different lasers were considered during the testing. Their basic properties can be seen on Table 4.1. Lasers were the only option for illumination, because they can create high power illumination for short time intervals.

Table 4.1 Some properties of the lasers used

Laser	Cavitar diode laser	Nd:YLF laser	Argon:Ion laser
Wavelength (nm)	690	527	488-489 and 511
Light beam	pulsed	pulsed	continuous
Safety class	4	4	3B

Laser light does not suit the illumination purpose until it has been processed. The processing is done by laser optics such as mirrors and lenses. The function of the laser optics is to guide the light from the laser to the illuminated subject and convert the light ray into a beam that covers the whole of area to be illuminated. Furthermore the intensity distribution of laser light can be smoothed using optics to give an even illumination of the subject. Different optics were used during testing depending on the laser used.

4.6.1 Effect of the wavelength on illumination

The wavelength of the laser has an effect on the illumination power. There are differences in the absorption coefficients of target surface depending on the wavelengths. Also the image sensor can be more sensitive to some wavelength than to others. In this work the illuminated object was a fresh wood sample with paint texture on the surface. In addition some water could condense on the surface of the sample. This kind of surface is very complex as it consists of hollow cells which are filled with air, paint and water. Furthermore the surface may deform during the compression. Throughout the testing it was observed that the short wavelengths seemed to give better illumination for wet wood samples than longer wavelengths.

It was concluded that the reason for different illumination properties for different wavelengths was the variation in the concentration of water in the samples. Clear water absorbs red light almost ten times more efficiently than green or blue light according to the study of Pope and Fry (Figure 4.6) [30]. It was concluded that water defines the light absorption properties for wet wood samples. That meant that by using a red laser light a lot of illumination power would be lost compared with using shorter wavelengths.

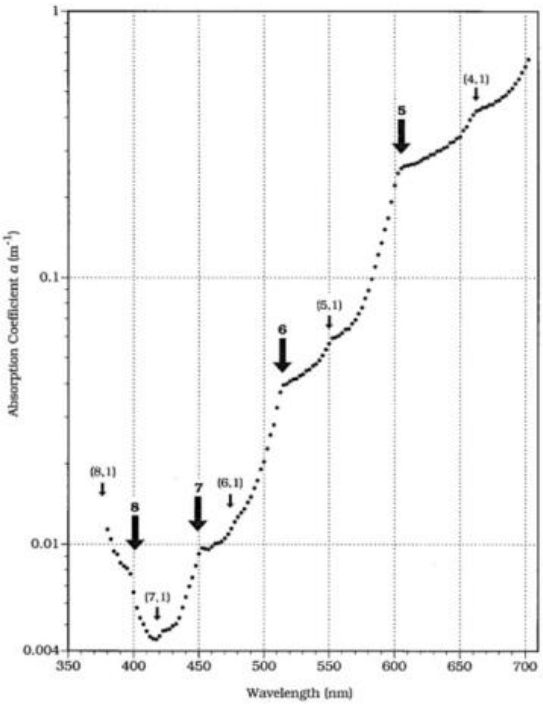

Figure 4.6 Absorption coefficient for pure water [30]

4.6.2 Choice of the illumination method

The illumination method was chosen to avoid the weaknesses. First of all the diode laser was eliminated. Its greatest advantage was small size for transport and an adjustable pulse length and repetition rate. However, at high recording rates it did not provide sufficient illumination power. This can be seen in the image taken of the wet test sample with a diode laser illumination. The image is shown in the Figure 4.7. It is clear that the test image on the left side is not sufficiently illuminated. The pulse length that was used in the taking of test images would allow a maximum of only 1000 fps.

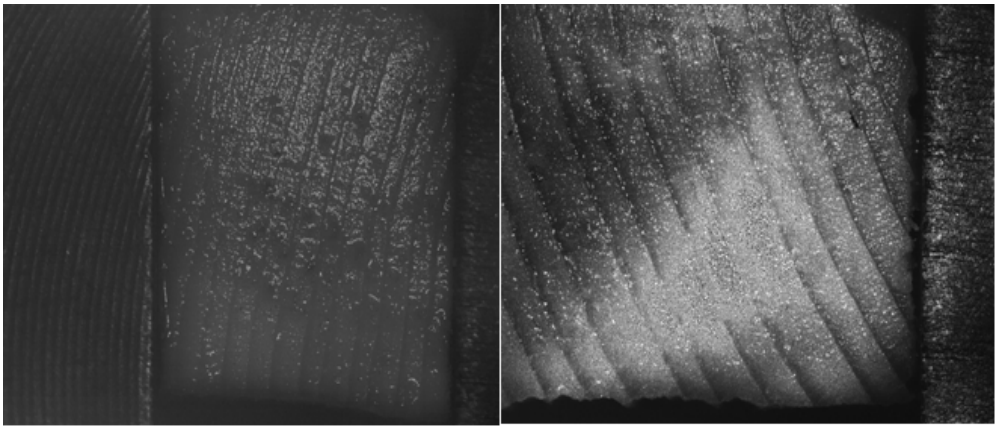

Figure 4.7 Test images taken with different illuminations. Left: Diode laser Right: Nd.YLF laser

The next illumination method that was eliminated was Nd:YLF laser. While it had enough illumination power, its maximum repetition rate was 20,000 Hz. During testing it was observed that the laser was not functioning correctly and a pulse rate of only 10,000 Hz could be attained. In addition to the limitation of the pulse rate the light intensities were not evenly distributed as can be seen in the right hand image in Figure 4.7. This caused part of the image to overexpose while other parts were not receiving enough illumination. The middle part of the image is overexposed, while the corners are still dark. The intensity pattern could be corrected using optical instruments, but the limitation in the pulse rate meant this laser could not be used in the measurements.

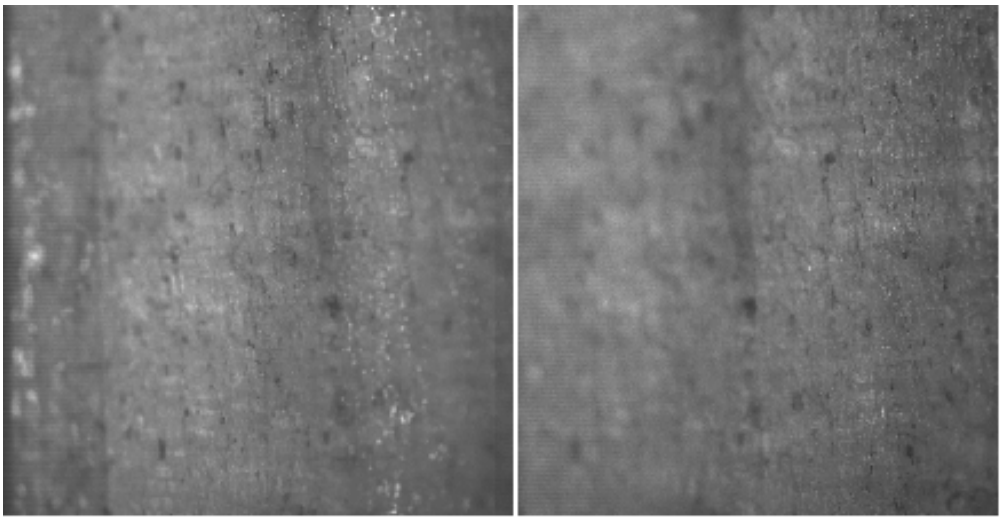

Figure 4.8 Two test images taken with Argon:Ion laser illumination with recording rate of 20000 fps.

The chosen illumination method was Argon:Ion laser. Figure 4.8 shows the test image taken with Argon:Ion illumination. It provided sufficient illumination for a recording rate of over 50,000 fps. The problem with the Argon:Ion laser was the motion blur, which would be caused by movement of the sample during exposure. As the laser created a continuous light beam the motion blur could be limited only by the camera shutter speed and recording rate. It was estimated that at recording rates of more than 50,000 fps motion blur would have such a small effect that it could be removed by good preprocessing of the images.

The optics that were used with Argon:Ion laser consisted of the optical fiber and diffuser optics. These optics belonged to a Cavitar diode laser, but after consulting with the manufacturer it was agreed they could also be used with the Argon:Ion laser. The optical fiber was used to guide the light and to scatter it so that the intensities were smoothed. The fiber was needed because the space for the recording equipment was very tight and the fiber allowed the illumination to be adjusted much more easily compared to moving the whole laser. The diffuser optics also smoothed the light intensity distribution and created the light beam from the laser ray.

4.7 Measurements

The measurements were conducted at the laboratory of Mid Sweden University at Sundsvall, Sweden. Before the measurements all the reflecting surfaces that were close to the sample in the split Hopkinson pressure bar were covered. The heads of the bars inside the device were painted black and the surface around the window was covered with black tape. These adjustments were made for safety reasons to avoid any reflections from the laser light. The block diagram of the recording set up is shown in Figure 4.9. The output from the strain gage transducer is connected to the trigger box, which converts the output signal on a TTL signal. The laser is not connected to the

computer or camera because it creates a continuous light beam and thus does not need to be synchronized with the camera. A pulsed laser would have been connected to the other equipments so that it could be synchronized with the camera.

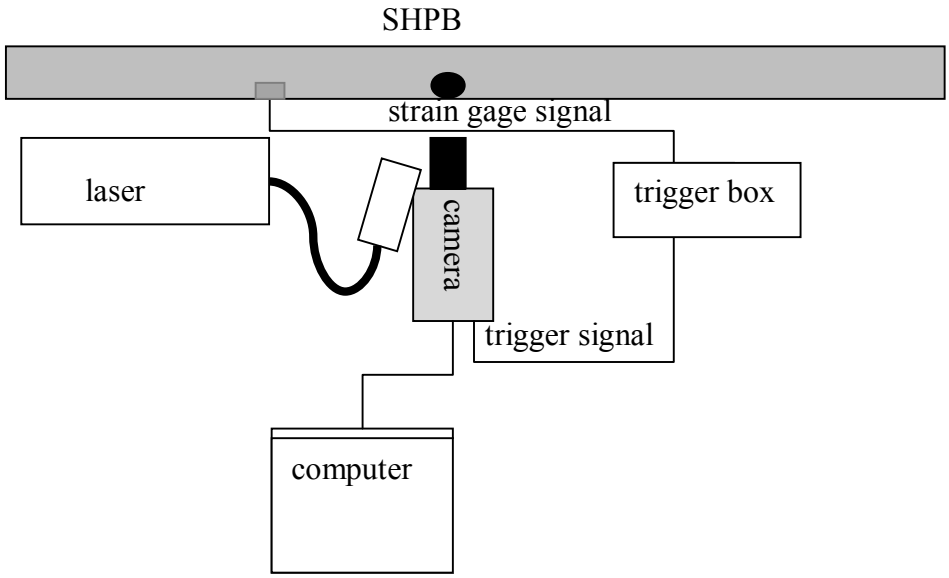

Figure 4.9 Block diagram of the recording set up

In Figure 4.10 the whole recording system can be seen with all the components in place. The camera is in the front and on the left are the laser optics and the optical fiber components. The cables attached to the camera are the power cable, the trigger signal cable, and the connection to computer.

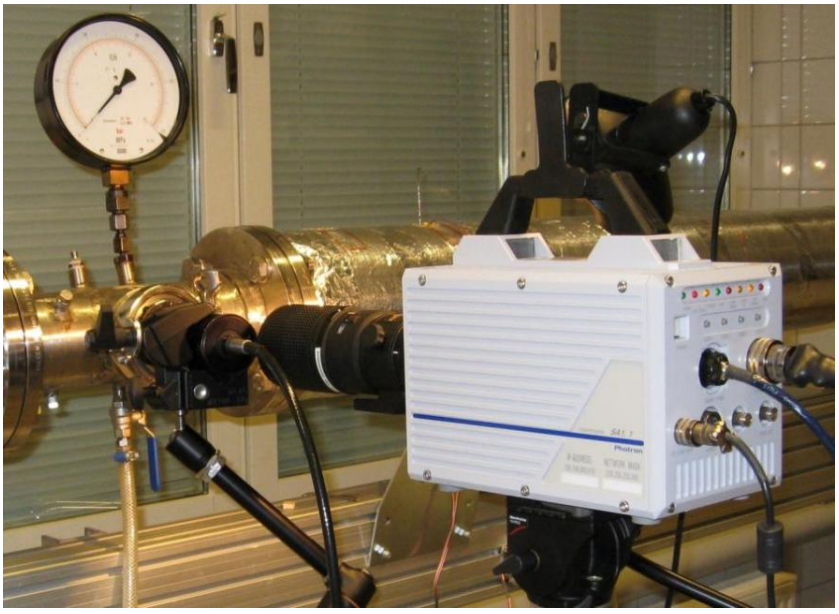

Figure 4.10 Picture of the recording set up

The functioning of the trigger system was tested before making the measurements. At the same time the final recording parameters were chosen. The final settings for the camera were a compromise between the sharpness of the image, the brightness of the image, the resolution, and the recording rate of the imaging system. It was concluded that 50,000 fps would be used as the recording rate for the camera. With this recording rate approximately 15 frames could be recorded during the first compression. The resolution with that recording rate was 448 pixels in width and 224 pixels in height. The camera shutter was adjusted to be open 1/99,000 spf, which gave us an exposure time of approximately 10μs. With this exposure time the images were sharp, and the illumination time was sufficient for the images not to be too dark. The trigger signal was adjusted to be on the 500th frame so there would be 500 frames recorded before the trigger. This was done as a precaution in case there should be a delay in triggering.

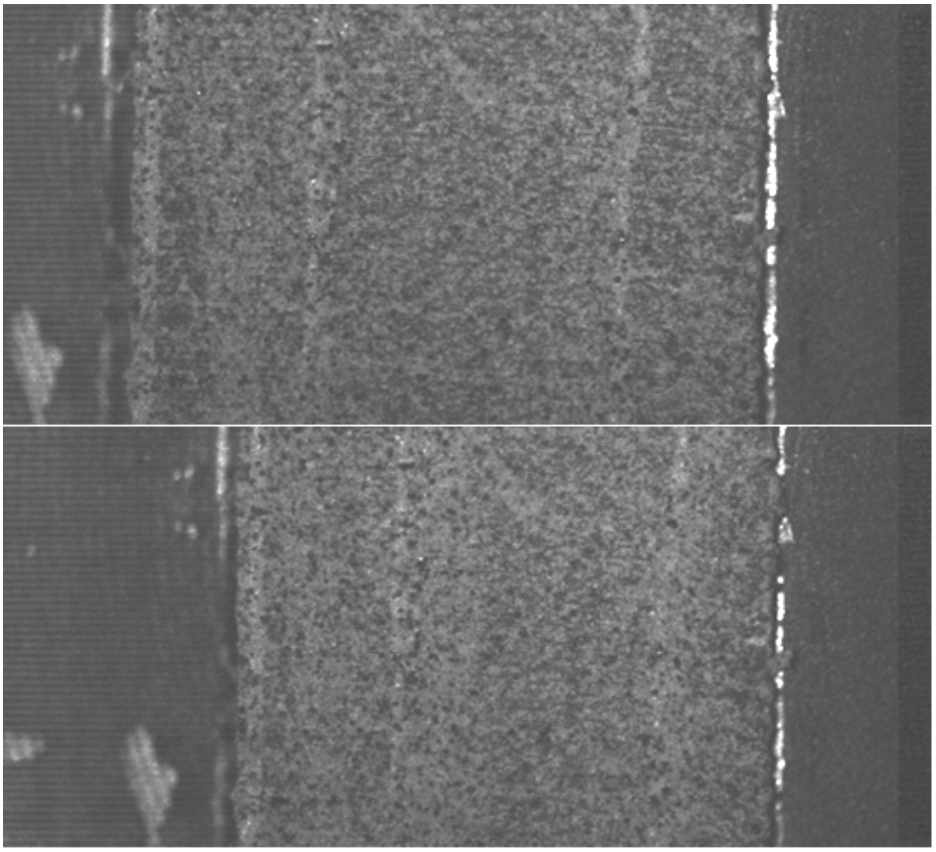

Figure 4.11 Frames taken before and after the compression from the room temperature measurements.

The high speed recording system worked and the quality of received images was adequate. In Figure 4.11 two typical frames from measurements are shown. The top frame is taken before the compression and bottom frame after the compression. The brightness and contrast of the frames was increased for better viewing. The actual frames were darker.

4.8 Problems during the image acquisition

During image acquisition there were several small problems that hindered the measurements. Some problems could be taken care of but a few of the problems were of the kind for which there was no solution. None of these problems were serious enough to prevent the image acquisition, but some image sets could not be used satisfactorily in the automatic analysis. The loading of only one sample was left completely unrecorded. This happened because the trigger signal was not received.

4.8.1 Spouting water

The samples used in the measurements were taken from fresh wood. Because of that they have moisture content of around 45%. There were a few extra samples that were dryer and few samples that had more moisture. Their moisture contents were 35% and 55% respectively. The problem with the moist samples was that during the compression the water inside of the samples would burst out of the sample surface. When the walls of the hollow cells that store part of the water collapse, the water inside the cells sprays out. The water would then block the view of the sample. In Figure 4.12 water can be seen spouting out from the three different places in the wood. These areas are highlighted in the image by white borders.

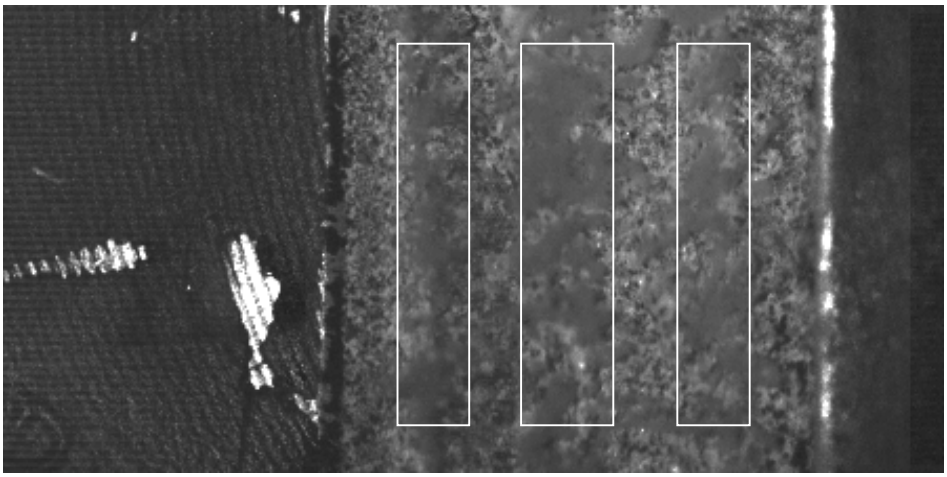

Figure 4.12 Water bursting out of a sample at three locations.

There was no solution to this problem as the moisture content of the samples needed to close to the moisture content of the fresh wood. In actual measurements it was observed that the water usually started coming out only after the first compressive pulse so it did not prevent the measurements. A few series of images could not be used in the analysis because the water blocked the view to the sample surface.

4.8.2 Boiling in samples

The moisture content in the samples also caused another problem. The water inside the samples and on the surface of the samples started to boil during the high temperature tests. This caused the samples to dry and the paint pattern from the surface was damaged. The destruction of the paint pattern can be seen in Figure 4.13.

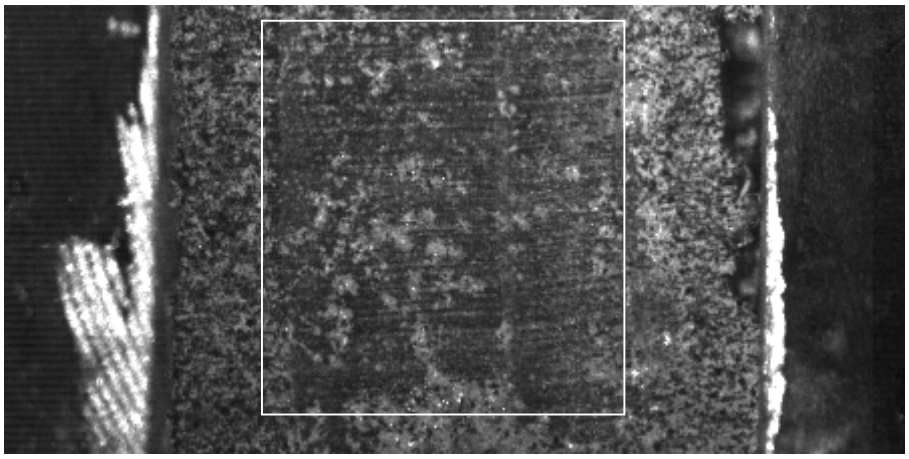

Figure 4.13 Destruction of the paint pattern in the middle of the surface of the sample

This kind of surface would not work as well in the correlation analysis as the original speckle pattern. There was no way of preventing this from happening, so the heating was done as quickly as possible to minimize the effect boiling. Initially it was thought that the samples could be covered with waterproof material that would prevent water from vaporizing. However, this idea was abandoned because the covering of the samples would create many additional problems for the measurements and any advantage that could be gained would be very small.

4.8.3 Condensing water

One problem that was considered in advance was that the hot steam used in the heating of the split Hopkinson pressure bar would prevent viewing of the sample. When the split Hopkinson device was warmed with hot steam, some water would condense on the window or on the surface of the sample and would cause distortions in the images. There were two methods to prevent the water from condensing on the window or on the surface of the sample. Firstly the window was heated with an electrical heater so that it would be warmer that the steam inside. This would prevent water condensing on the window.

The other method was to raise the temperature inside the device above the required temperature by approximately 10 ºC and then the temperature was rapidly dropped to the required point. That cleared the condensed water from both the window and from the sample.

4.8.4 Thermal expansion

The thermal expansion caused a few problems during the measurements, but it did not affect the image acquisition. The position of the bars in the device changed slightly when the temperature rose, because the gas gun and the striker bar were not heated. Because of this the striker bar must be separately adjusted each time so it would hit the incident bar.

Raising and dropping the temperature inside the vessel caused another problem. When the temperature started to decrease, a small gap appeared between the bars and the sample because the lowering the temperature caused the bars to shrink. In one case the gap became so large that the sample fell out of position. Since that incident a manual load wad applied to the incident bar when the temperature started to drop in order to fix the sample between the bars.

4.8.5 Trigger problems

The hot steam caused problems with the triggering system of the camera because the wires from the strain gage transducer in the incident bar were affected by the steam. The heating caused so much noise in the strain gauge transducer signals that the trigger signal would be sent to the camera continuously thus making actual triggering impossible. In the end the trigger signal for the camera was taken from the other strain gage transducer in the receiver bar. The timing for the trigger was not as accurate when taken from the receiver bar as it was when was taken from the incident bar, but it was sufficiently accurate as a large margin of error for triggering was permissible.

5 Image analysis algorithms

The goal for image analysis was to determine the local strains inside the samples using the recorded data sets. To measure the strain the deformations that took place in the specimen between consecutive images must be defined. There are several known algorithms for computing the local displacement vectors between two images. These algorithms use cross-correlation functions to find the displacement of the sub images in consecutive frames. It is assumed that the deformation within each of these sub images is so small that the corresponding sub image can be found from the next frame. The full deformation is found by combining these local displacements and the local strain can be computed from the relative displacements of the sub images.

Cross-correlation analysis requires that there is some random texture pattern in images so that the consecutive frames are strongly correlated. Furthermore, the deformation between consecutive images must be sufficiently small that the correlation between sub images is not lost. Some additional analysis algorithms were tested in case the image recording did not yield good enough image sets for a correlation analysis to work. These methods were based on a calculation of the thickness of the layers of the growth rings. With that kind of approach only two images would be needed and no extra texture needed to be added into the samples. The images would be taken right before and after the deformation. The change in the thickness of the layers would give the average strains in early wood and late wood layers in the direction of the compression. As the recordings were successful these algorithms are only presented briefly.

5.1 Recorded images

The images that were used in analysis had a resolution of 448*224 pixels. Each pixel had a grayscale value between 0 and 255 to represent the intensity of light at that location. The value 0 would correspond to black pixel and 255 to a white pixel. The values between the 0 and 255 represented different shades of gray. A typical image for analysis is shown in the Figure 5.1. It shows the wood sample between the metal bars. This sample has three growth rings as can be seen from the number of bright late wood layers.

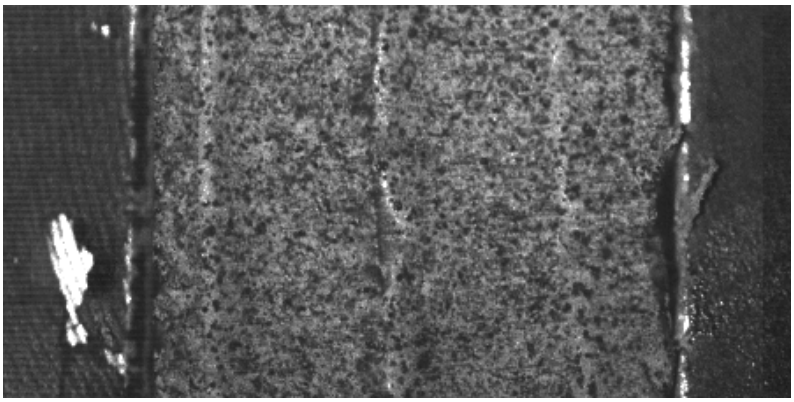

Figure 5.1 Grayscale image frame from the measurements

The analysis is undertaken using only the middle part of the image where the sample is. The area of interest will vary from one test set to other because of variation in the sample size. The area of interest covers the whole sample in horizontal direction. In a vertical direction a small margin of image is excluded at top and bottom.

5.2 Preprocessing of recorded images

Preprocessing is carried out to enhance the image quality and to highlight the required properties in the recorded image sets. With good preprocessing the results will be more accurate and the computational time for the algorithm can be reduced. Typical preprocessing procedures are removing the noise caused by the camera, removing the background and unwanted objects, correcting the illumination intensity changes either in one image or between consecutive images, enhancing the contrast in the image, and sharpening the images. The choice of preprocessing procedures depends on the actual images

In this work the goal for preprocessing was to remove any artificial noise caused by the camera. This kind of noise consists of single pixels and can be effectively filtered away by median filters. A median filter is a nonlinear filter and the output of the median filter is defined by ordering the values inside the filtered area in descending order and choosing the middle value to be the output. This procedure is repeated for each of the pixels. The size of the median filter is chosen according the noise. A larger filter will remove noise more efficiently than a smaller one, but it can also filter out significant details from the image.

Another image enhancement procedure that can be implemented is normalizing of the intensity changes. This is done if, in one image, the illumination conditions change locally or for whole images if the illumination changes between different images. If the intensities of the image are distributed on a very narrow band of gray scale values, the contrast in the image can be increased.

5.3 Interpolation methods

Interpolation is used in image analysis to acquire sub pixel accuracies in calculations. Interpolation means computing new values for locations between known points by using the information of the values at the known points. Interpolation can be done in many ways depending on the required accuracy and the computational efficiency.

The simplest of all interpolation methods is nearest neighbor interpolation. In nearest neighbor interpolation the new value for each location is the same as the value of the nearest pixel.

Bilinear interpolation yields a much better estimate and is a more useful method for interpolation. The value of point (*x, y*) between four pixels is calculated using two linear interpolations. First the linear interpolation is computed in a horizontal direction to calculate two interpolated values and then using these two values the interpolation is conducted in the vertical direction. The new value in bilinear interpolation is calculated as a weighted sum of intensity values. The weights depend on the distance from the new location to the known points. The linear interpolation in is defined as in equation

$$f(x) = \frac{x_2 - x}{x_2 - x_1} \times f(x_1) + \frac{x - x_1}{x_2 - x_1} \times f(x_2), \tag{6}$$

where $f(x_1)$ and $f(x_2)$ are values at the known locations and the unknown location x is in between them. With bilinear interpolation a continuous intensity pattern can be calculated for an image.

In bi-cubic interpolation the new value for sub pixel locations is calculated using the information from the two nearest pixels in each direction so total area of 4*4 pixel values is used. The interpolated value is computed with the equation

$$p(x, y) = \sum_{i=0}^{3} \sum_{j=0}^{3} a_{ij} x^i y^j . \tag{7}$$

The interpolation procedure consists of determining the 16 coefficients a_{ij}. The coefficients are determined using the intensity values at the four nearest pixels and the derivatives or their estimates at these locations. Bi-cubic interpolation yields best estimates for sub pixel locations as it has both continuous intensities as well as continuous derivatives if the coefficients are determined properly. However, it is computationally much more intensive compared to the other interpolation methods.

5.4 Segmentation of earlywood and latewood layers

Several methods were considered for use where fast enough recording rates could not be attained. In these cases the best way to perform the analysis would be to use just the images taken before and after the deformation. Instead of following through the whole deformation, the thickness of each early wood and late wood layer would be calculated at the start and the end positions. The differences in these thicknesses could be used to calculate the average strain in each layer in the direction of compression. In this way the average strain could be defined for each layer of the growth ring. Only the strain in the direction of the compression could be defined.

The only thing the algorithm needed to do was to segment the early wood and the late wood layers. This, however, proved to be a very hard task, especially for moist samples. The most common problem was detecting the edge in the transition wood that grew in the middle of the growing season. At this location the change from the earlywood to latewood is gradual. Another problem was the brightness changes in the wood. In the locations where the deformation took place, the wood material became denser and slightly darker and this can cause errors in the detection of the edges.

Two types of algorithms were tried. The first ones tried to separate the layers by using a threshold value to separate intensity values. The task was to find suitable threshold value. The other method tried was to segment the image into earlywood and latewood segments by finding the edges between the layers. The edge detection is based on locating the large local changes in the intensity values.

5.4.1 Thresholding algorithms

The first method to be considered used the threshold value to separate the wood layers. Because the early wood is lighter than late wood, separating them by using the threshold should be possible if the threshold value can be chosen correctly. However, a global threshold value cannot be used as the color of the wood varies between different growth rings and the color differences between different layers in the moist samples are small. In addition, the edges should be detected very accurately as error in edge location leads to large error in the strain measurements in the wood layers. Using a local threshold requires a different threshold value for each pixel or small area of pixels.

There are several different ways defining the local threshold values. Two different ways were tried. The first was to define the local threshold was using the mean of the intensity values in a window around the pixel as a threshold value. The window used should be large enough so that each window includes both early and late wood. In this way the threshold value should be between the intensity values of the two different layers. The second way to define the local threshold value is first to compute the global mean I_g of the intensity values and the adjust it by averaging it with the local mean of intensity values I_l.

5.4.2 Edge detection algorithms

There are many ways of detecting the edges of the images. Here the gradient information was tested. The image was first smoothed to eliminate noise. Then the gradient in the direction of the x-axis were computed. The locations of the peaks and troughs in the gradient values represent the edges. They can be computed taking second gradients in the same direction. The locations of zeros then correspond to the edges. This method, however, did not work as despite the use of different smoothing filters the gradients were too noisy for any useful information to be retrieved.

The other method tested for edge detection was RMS (root mean square) filtering. The filter size was 3*3 pixels. At each location the RMS of deviations from the local mean value is computed. In the filtered image the highest values represent the edges in the original image. This image can then be turned into a binary image by thresholding. The RMS filtering found edges better than gradient search method, but the results were not nearly good enough for use in the analysis.

5.5 Correlation based algorithms

Image correlation is a way of using image analysis to define deformations in the specimen. There are several ways how the correlation can be used. The basic requirement is that there must be at least two images taken during the deformation of the specimen, which have some kind of random surface pattern that could be tracked. This pattern can be either different colors or intensities or small surface shapes. If the specimen has no suitable pattern on the surface, it can be added, for example, by spraying a little paint on the surface from a distance.

The first image is the reference images and is taken before the deformation. The second image is taken after a small deformation has changed the surface of the specimen. From the reference image the grid of control points or nodes is chosen. Local areas around these points are called interrogation windows and they are used as reference areas for correlating. A cross-correlation function is used to find the best matching area in the second image for each interrogation window. The best match has the highest correlation and the location of the best match defines the displacement of the interrogation window.

5.5.1 Cross-correlation functions

Cross correlation functions are used to determine the similarity of two signals when one of them is delayed with different time intervals. The signals can be either one- or multidimensional. In image analysis cross-correlation can be used to detect small displacements of local areas. When the cross-correlation is computed for corresponding areas in subsequent frames, then the correlation coefficient can be computed for each shift.

The highest correlation coefficient indicates the best match and thus the location of the highest coefficient defines the amount of the shift that the area will move between the frames. In the case of very large shifts some initial estimation of the shift must be used so that cross-correlated areas can be located sufficiently close to each other. An example of a clear correlation peak is shown in the Figure 5.2.

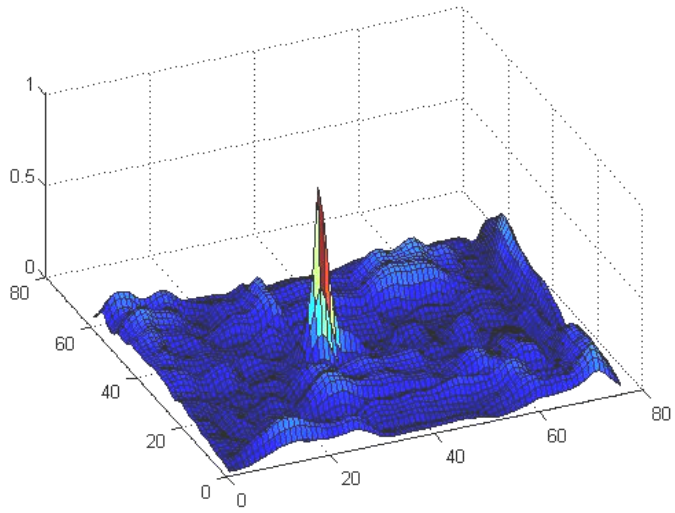

Figure 5.2 Correlation peak

There are several cross-correlation functions that can be used to determine the correlation coefficients. They will each yield slightly different results depending on the case. Furthermore, computing time for some of the functions varies. This could be the deciding factor when the amount of the data to be analyzed is large.

The standard cross-correlation *C* is defined in the equation

$$C = \sum_{i,j} \left[F(x_i, y_j) * G(x_i^*, y_j^*) \right], \tag{8}$$

where the *F* and the *G* are the intensity values of two areas in the consecutive frames. The values of the standard cross-correlation can be calculated more quickly by using FFT. The requirement is that the interrogation areas *F* and *G* are square shaped and the length of each side is 2^n. The problem with standard cross-correlation is that it does not take into account intensity changes. This is why a bright area gives a higher correlation than an exactly matching area. This problem is corrected in normalized cross-correlation.

Normalized cross-correlation C_n is defined in the equation

$$C_n = \frac{\sum_{i,j}\left[F(x_i, y_j) * G(x_i^*, y_j^*)\right]}{\sqrt{\sum_{i,j} F(x_i, y_j)^2 \sum_{i,j} G(x_i^*, y_j^*)^2}}. \quad (9)$$

Normalized cross-correlation requires more computational time than standard cross-correlation, but it can also be computed more efficiently using FFT, with the same restrictions as in the case of standard cross-correlation. However, compared to standard cross-correlation the normalized cross-correlation removes the effects of the intensity changes between different frames. The normalized cross-correlation function can still be modified by removing averages from each intensity value. Such a correlation function is represented in the equation

$$C_r = \frac{\sum_{i,j}\left[F(x_i, y_j) - \bar{F}\right]\left[G(x_i^*, y_j^*) - \bar{G}\right]}{\sqrt{\sum_{i,j}\left[\left(F(x_i, y_j) - \bar{F}\right)^2\right]\sum_{i,j}\left[\left(G(x_i^*, y_j^*) - \bar{G}\right)^2\right]}}. \quad (10)$$

Usually the location of a correlation peak needs to be defined with sub pixel accuracy. The discrete values for peak location do not give sufficient accuracy. There are several methods for defining spatial location of the peak in sub pixel accuracy. The simplest methods are curve fittings.

5.5.2 DIC (Digital Image Correlation)

Digital image correlation (DIC) is the best known of the image analysis algorithms for strain calculation. It was originally suggested by Sutton and coworkers [7], but the method has since been refined on many occasions for improved accuracy and performance [8,9]. DIC finds the best match for the interrogation area by minimizing the correlation function iteratively. The DIC algorithm works well if the deformations inside these areas are nearly homogeneous. The DIC algorithm is described briefly below.

The initial hypothesis for DIC is that the intensity values do not change during the deformation. Only the distribution of the intensity values will change. Thus for each interrogation area there is a corresponding area in the next frame. These areas are linked by the deformation. The arbitrary area of intensities *F(x, y)* in the first image can be found in the second deformed image as a *G(x*, y*)*. These areas are connected by deformation *D*. This deformation can be seen on Figure 5.3.

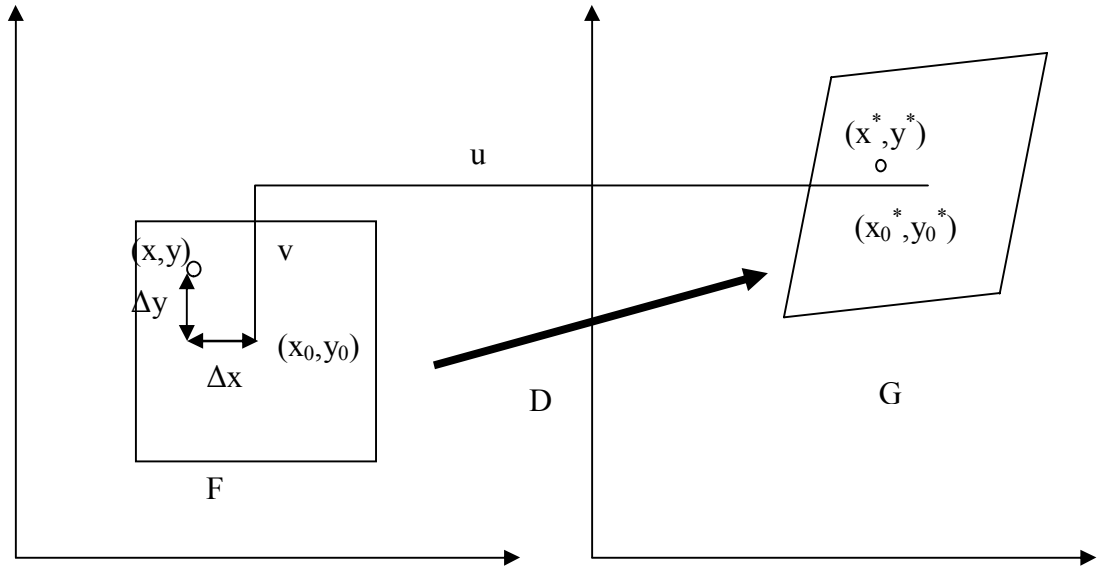

Figure 5.3 Area F is connected to area G by deformation D

The deformation can be represented as a movement of an arbitrary point (*x, y*). If the centre point of *F* is (x_0, y_0). The points are mapped into the deformed image at other locations using the equations 11 and12.

$$x^* = x + u + \frac{\delta u}{\delta x}\Delta x + \frac{\delta u}{\delta y}\Delta y \tag{11}$$

$$y^* = y + v + \frac{\delta v}{\delta x}\Delta x + \frac{\delta v}{\delta y}\Delta y \tag{12}$$

In equations where $\Delta x = x - x_0$, and $\Delta y = y - y_0$ are the distances of the arbitrary point from the centre of the area. The values u and v are the displacements of the centre point (x_0, y_0) in x- and y-direction respectively. $\delta u/\delta x$, $\delta u/\delta y$, $\delta v/\delta x$ and $\delta v/\delta y$ are the displacement gradients. They describe the relative movement of an arbitrary point compared to the centre point. Their effect to the shape of the grid is illustrated in Figure 5.4. It can be seen that $\delta u/\delta x$ is the local strain along the x-axis. Similarly $\delta v/\delta y$ is the local strain along the y-axis and $\delta u/\delta y$ and $\delta v/\delta x$ are the components of the shear strain.

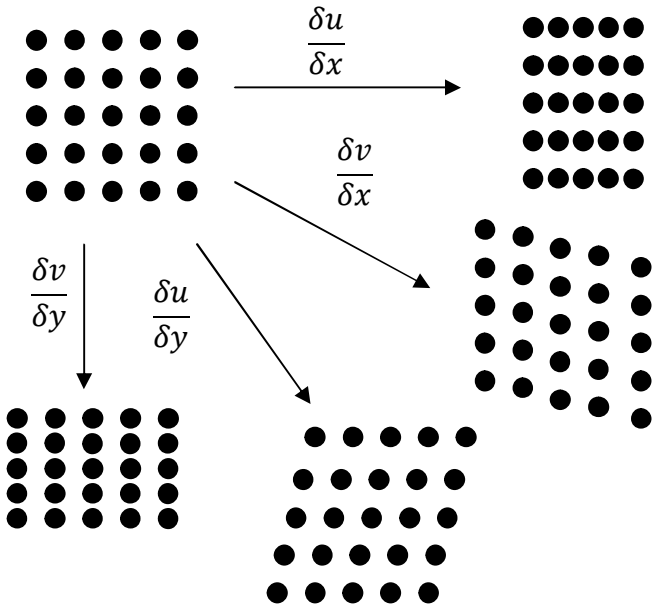

Figure 5.4 The effect of displacement gradients on the shape of the area

The problem is finding optimal values for displacements and displacements gradients so as to minimize the correlation function, which is defined in equation

$$s\left(u, v, \frac{\delta u}{\delta x}, \frac{\delta u}{\delta y}, \frac{\delta v}{\delta x}, \frac{\delta v}{\delta y}\right) = 1 - \frac{\sum_{i,j}[F(x_i, y_j)][G(x_i^*, y_j^*)]}{\sqrt{\sum_{i,j}\left[\left(F(x_i, y_j)\right)^2\right] \sum_{i,j}\left[\left(G(x_i^*, y_j^*)\right)^2\right]}}. \quad (13)$$

The normal way to minimize the correlation function is to use an iterative optimization method such as that of Newton-Rhapsod for multi variable problems. It converges quickly to a minimum value if the initial guess is close. A good way to approximate the initial displacement is to use the cross-correlation function without the deformations. The displacement gradients are set to zero at the beginning of the iterations. For th Newton-Rhapsod method, the first and second order derivatives for the correlation function is needed to be computed. Instead of using discrete intensity values interpolation is used to generate a continuous intensity pattern. [7, 8, 9]

In their research H. Lu and P.D Cary suggested using second order displacement gradients [31]. This increases the number of parameters to be optimized and would yield much more accurate mapping of the deformation and thus a larger interrogation window could be used. However, if the optimization of six parameters is increased to optimization of 12 parameters, this leads to a more complex algorithm and longer computational time.

5.6 The algorithm used

The analysis algorithm was computed on the MATLAB. The basic problem was to find good matches in the locations where the deformation took place. As the local deformations were large inside the interrogation windows, the DIC algorithm was not good at modeling the deformation. Adding more deformation parameters would allow better modeling of the deformation but at the same time a larger window size is required and the computational time would increase. For these reasons a simple algorithm was chosen and the deformations inside the interrogation areas were not taken into account in the algorithm. The match for each interrogation area was found by multiple correlation passes with decreasing window size. In this way the algorithm was fast and the high correlation peak values between interrogation areas could still be found.

5.6.1 Overview of the algorithm

The analysis of the images was completed by following the movement of the control points. Control points were chosen in such a manner as to form a rectangular grid on top of the sample in the first frame. The movement of these points is followed from one frame to the next until the final locations for all the control points had been identified. Each displacement is defined by cross-correlation. The sub image around the control point is cross-correlated with the corresponding sub image in the next frame. The spatial location of the peak amongst the correlation coefficients defines the displacement of the sub image between consecutive frames. Two passes of cross-correlations was used to increase the accuracy in computation of the displacements. In addition the final location of the correlation peak was defined with sub-pixel precision to further increase the accuracy.

In the algorithm used the best match for each interrogation window is found from the consequent image using two passes of cross-correlation matching. In this algorithm the first correlation is used to make an initial estimate of the displacement using a large interrogation window. This estimate can be used to accurately locate a new, smaller search window to the second image. The second pass uses a small interrogation window to find a more accurate value for the displacement. This displacement value is computed with sub-pixel accuracy. After all the displacements between two subsequent frames have been computed, some further post-processing is carried out. Post-processing consists of median filtering to remove inaccurate displacement estimates and to smooth the displacement vector field.

The final local strain values are calculated from the relative movement of the control points. Deformations take place at locations where the distance between subsequent control points change. The local strain values can be calculated along both the x-axis and the y-axis.

5.6.2 Grid of control points

The grid of control points was chosen from the reference image. The size of the grid was chosen to cover the specimen in a horizontal direction, because the strain values in that direction were the main point of interest. In a vertical direction a margin was left at both at the top and bottom to simplify the computations. The size of the grid varied a little because the size of the samples varied. Figure 5.5 shows the grid of control points plotted on top of the sample at their starting locations.

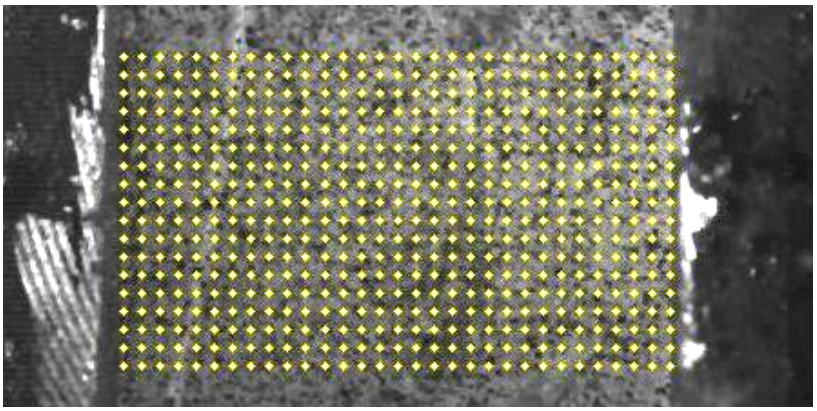

Figure 5.5 Grid of control points at the start of the analysis

The density of the grid was chosen in such a manner that there were several points inside each layer of the growth rings. In this way the strain differences between the different layers of the growth rings could be determined. Furthermore, the changes in the strain a within layer could also be determined. On the other hand, too dense a grid would increase the computational time of the algorithm. In addition, strain calculations for very small areas could have large errors as the small errors in the displacements of the control points could accumulate. The density of the grid was varied between 5 and 15 pixels to determine the optimum value. Finally, the density of the grid was set at 10 pixels in both directions.

5.6.3 Displacements vectors

The displacement of the individual control point between two frames is defined by multi pass cross-correlation analysis. In multi pass analysis the size of the interrogation window around the control point is reduced as the estimation of the displacement becomes more accurate. The initial estimate of the displacement is done using a large interrogation window size. This estimated displacement is then used to find a new search location for a smaller interrogation window. A smaller window is used in the second search so that the effect of the deformations can be minimized. This process can be repeated as many times as needed but normally two passes are sufficient. The size of the windows is chosen according the application.

In this work the first window was 32*32 pixels in size. It was correlated with a slightly larger search area. The search area was longer in the direction of compression. This was done to compensate for the fact that there was higher movement on the left side of sample. Using a large search area allowed finding correlation values to be found. These higher correlation values came at the cost of increased computational time. The second window was 16*16 pixels in size. A smaller window size could not be used as the speckles on the surface of the specimen were too large. The correlated area needs a distinguishable gray scale pattern and for that reason several speckles need to be within the correlated area. The cross-correlation function that was used was a normalized cross-correlation. The correlation function is shown in equation 10.

The location of the correlation peak from the second pass of correlations is determined with sub pixel accuracy. It is necessary to define the displacements at sub pixel accuracy as otherwise the small inaccuracies in displacement vectors could accumulate when the analysis is done across a large number of frames. In this algorithm, the sub pixel accuracy was attained using interpolation. 5*5 surroundings of the correlation peak was interpolated using bi-cubic interpolation. More accurate location of the peak was found from the interpolated values. The location of the peak was determined with an accuracy of 0.1 pixels.

5.6.4 Post processing of displacement vector field

Once all the displacements for control points between two frames had been calculated the displacements were checked and errors removed. Because almost all the movement takes place in the direction of the x-axis, the displacements of each column of the grid points should be close to each other. The largest deviations are removed by comparing each displacement to the median displacement value within its own column. If the difference was too large in either x- or y-direction that displacement is replaced by the median value. After this correction the median filter was applied to the displacement values.

5.6.5 Strain calculations

After each frame when the new displacement values were added to the location of the control points, local strain values were calculated. The strain values could be studied as a time series. The strain values were calculated in the direction of the x-axis. In addition, the strain along y-axis and the shear strain could also be calculated, but in this work the strain values in the direction of the compression were the values of main interest. Figure 5.6 shows an example of the grid of control points at their final locations.

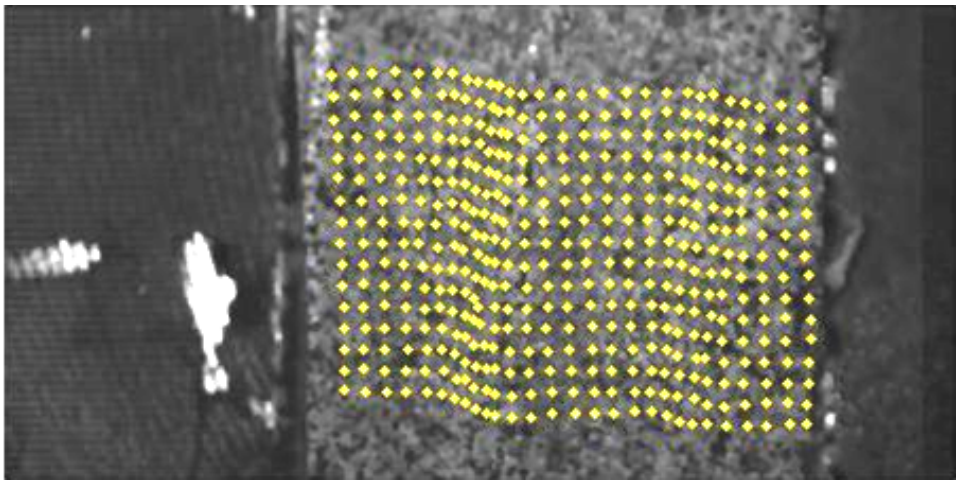

Figure 5.6 Final locations of control points

The strain value was computed for each area constrained by 2*2 control points. At the beginning these points were at a distance of 10 pixels from each other in the shape of a square. After the deformation, the area defined by control points is no longer square but it has became quadrilateral. An example is shown in Figure 5.7, where the corners of the shapes represent the four control points.

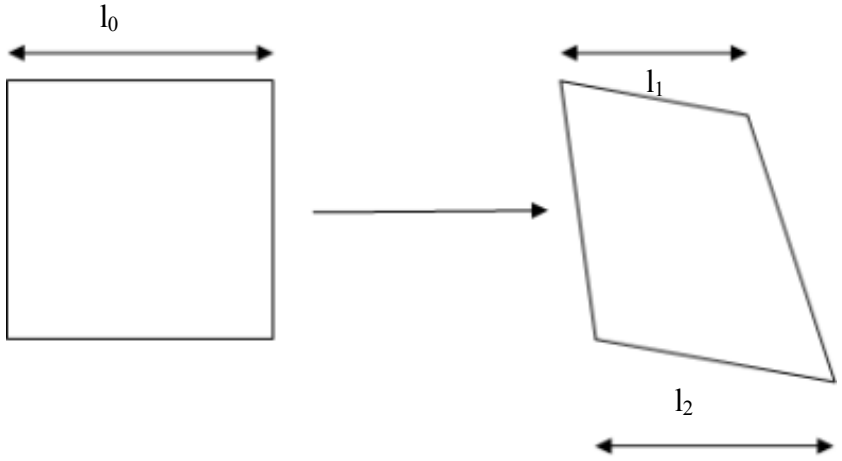

Figure 5.7 Changes in the length of the square area

The strain in the direction of the x-axis is calculated with the equation

$$\varepsilon = \frac{\frac{l_1 + l_2}{2} - l_0}{l_0}, \tag{14}$$

where l_1 and l_2 are the lengths in the direction of the x-axis of the upper side and the lower side of the final area in respectively. The final length of the area is defined as a mean of the l_1 and l_2.

5.6.6 Output of algorithm

The algorithm stores the location of the grid after each frame so the strain values can be calculated for any time particular intervals. The grid and local strain values were plotted after each frame to observe the functioning of the algorithm. The grid was plotted on top of the image frame. The strain values were plotted both as contour plots (Figure 5.8), where the image is divided into regions, that have different strain levels and as a strain surface map (Figure 5.9).

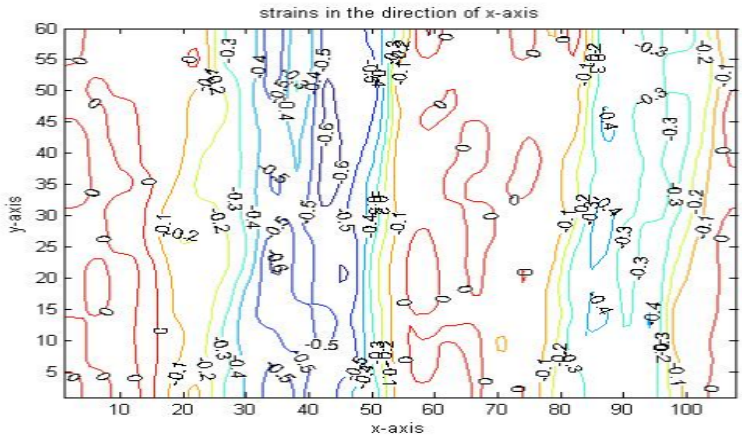

Figure 5.8 Strain contour map

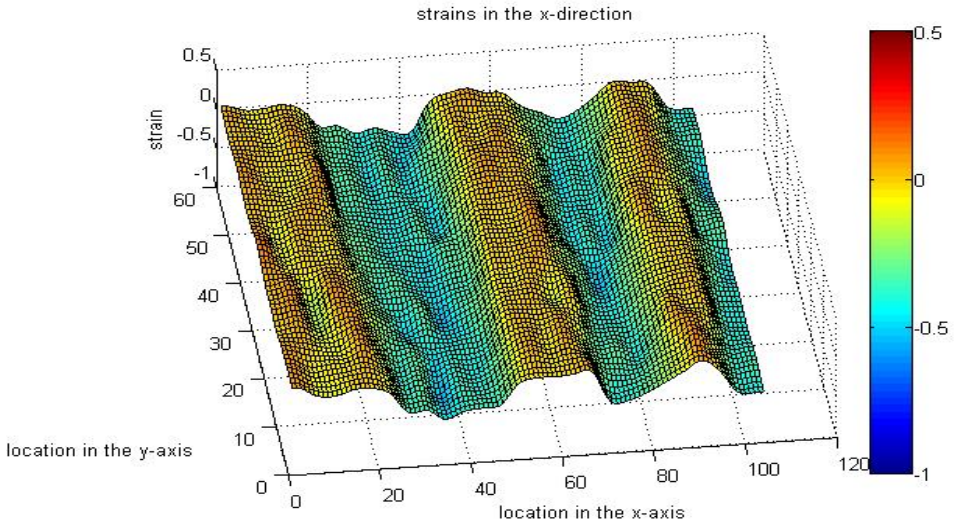

Figure 5.9 Strain surface map. The color indicates the strain level. High compressive strain is shown in dark blue and no strain shown in yellow

In the contour plots the contour lines were chosen with values from -1.0 to 0.1 with increments of 0.1. Using denser line intervals would make the plots tangled. Strain values were interpolated using bi-cubic interpolation to generate a smoother image, because there was only one value for each local area defined by the control points.

5.7 Accuracy and errors of the algorithm

The accuracy of the algorithm depends on the correlations. High correlations are attained if the images have distinctive gray scale patterns and the movement and deformation between consecutive frames is not large. In a case where there is no deformation at all and the only changes between frames are displacements, the correlations are high if the search area has been chosen correctly. Large deformation causes the biggest problems for the algorithm.

There is some bias towards integer valued displacements. This effect is called the peak locking effect. Although the location of the correlation peak is computed in sub-pixel accuracy using bicubic interpolation in the region around the correlation peak, the sub-pixel part of the displacement will be weighted towards zero displacement.

The test data for the algorithm consisted of series of constant images. These series were used to test the noise level of the algorithm. The calculated displacements are shown in the Figure 5.10. The distribution is very narrow as was expected in the case of zero displacements.

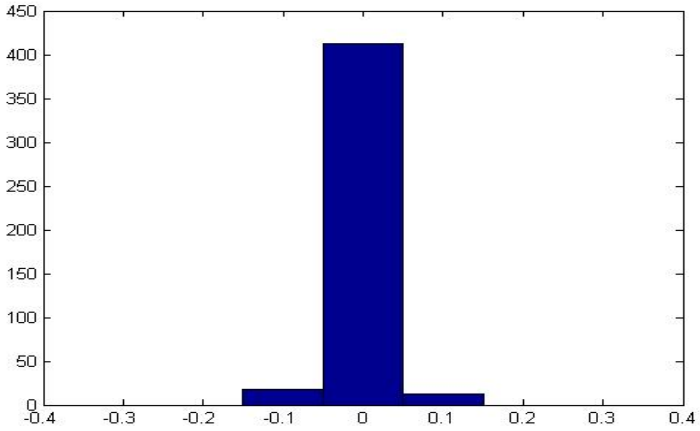

Figure 5.10 Histogram of the calculated displacements between constant images

The second set of test data consisted of images with constant displacements. They were created from the measured data by shifting the columns of a chosen frame to the left by a constant number of pixels. As long as the displacements were relatively short compared to window size and search area, the calculated displacements had the same kind of distribution as in case of zero displacements.

When the displacements between the two images were several pixels longer than the search area, the performance of the algorithm dropped. In that case perfect matches for pattern in the first frame could no longer be found from the search area. That meant that the correlation values were lower so the probability of errors increased. The post processing of displacement vectors was able to correct most of these errors.

Final tests should have been made for images where there was a known level of deformation. However, there was no test data available that would model known deformations. Deformation lowers the performance of the algorithm as correlation values are lower. A number of tests would be needed to see the actual impact of deformation as there are many ways in which the deformation can take place. Testing with images that show known deformation needs to be done at some point to verify the performance of the algorithm.

6 Local strain levels in the wood

The purpose of the analysis was to get an idea of what happens inside the wood sample during high strain rate compression. The main goal was to compute strain distributions at a sufficient level of accuracy. This meant detecting regions with higher strain levels and comparing their locations with the position of the growth rings in the original sample. Smaller details, such as narrow strain peaks, were not analyzed.

In this work the local strain distributions were calculated for eight samples of all 44 measured samples. These samples were chosen to represent different test temperatures and fatigue levels. The image quality was a factor when the samples for analysis were chosen. The number of samples analyzed is not sufficient to draw statistically proof conclusions but the results can be seen as indicative. An additional problem for conclusions is the variation between the samples. Samples were different in size and the number, thickness, and orientation of the growth rings varied.

6.1 Local strain distributions in samples

The chosen samples are shown in Table 6.1, where their fatigue levels and testing temperatures can also be seen.

temperature (°C)	Fatigue level			
	no fatigue	low (6000)	medium (12000)	high (20000)
130	B-5-5-4		A-1-11-5	A-1-12-2
100		A-1-3-2		
60		A-1-10-5		
20	B-1-12-3		A-1-20-5	B-1-4-3

Table 6.1 The samples analyzed

The results are presented as strain maps, where regions of different strain levels are separated by the contour lines. The strain levels for regions are from 0.0 to -1.0, with an interval of -0.1. The strain values have been computed in the direction of compression, which is also the direction of the x-axis. For each sample, two strain maps are presented. The first figure shows the strain values in the direction of compression during the whole of the compression. The second figure shows the strain values from start of the compression to the middle point of the compression. This second figure is shown to illustrate the accumulation of the strain.

All the strain values are negative because the deformation is compressive. The absolute value of the strain value shows the magnitude of the deformation. Because these strain values are computed in the direction of compression they are not a measure of total strain. Total strain values could be defined by also taking into account the strain in the direction of the y-axis as well as the shear strain.

6.1.1 Sample B-1-12-3

Sample B-1-12-3 was tested under the reference conditions so it had no applied fatigue and the test was performed at 20 °C. The sample had two latewood layers that are marked in Figure 6.1 with white arrows. Due to the painting, the growth rings are not clearly visible but the densest part of the latewood can still be distinguished. The samples were oriented in such a manner that the direction of the compression is same as the direction of the radial growth.

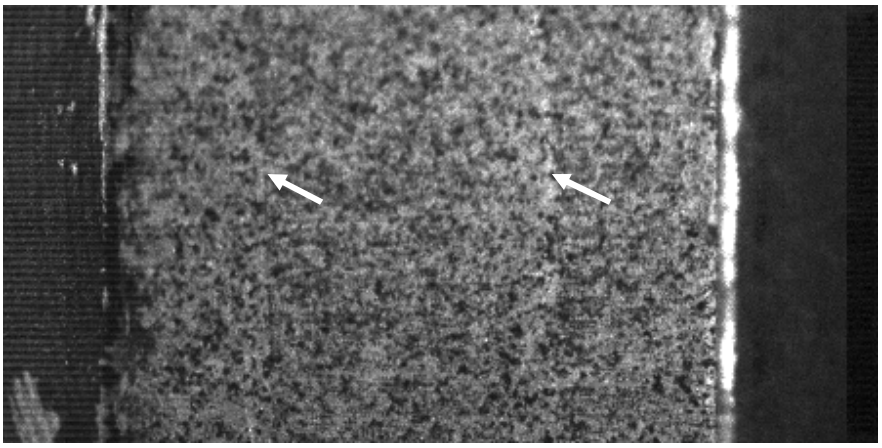

Figure 6.1 Growth rings of sample B-1-12-3

The total strain distribution and middle strain distribution are shown in Figure 6.2 and Figure 6.3 respectively. In Figure 6.2 strain values are computed over the whole compression during the first pulse and in the Figure 6.3 the strain levels are computed from the start to the middle of the compression to see how the strains accumulates during the deformation. The strain in the sample is concentrated on two regions. The first region is around 3 mm along the x-axis and the second region is around 5 mm. In other parts of the sample strain is close to zero. The first strain region covers the area from 2.0 mm to 3.5mm. The strain in that region varies mostly around -0.3. At the highest level small peaks of over -0.5 were detected. The second region covers the area from 4.5 mm to 5.5 mm so that region is narrower, but the strain in that region is higher. The strain is around -0.6. Lower strain levels are only located near the edges of the area.

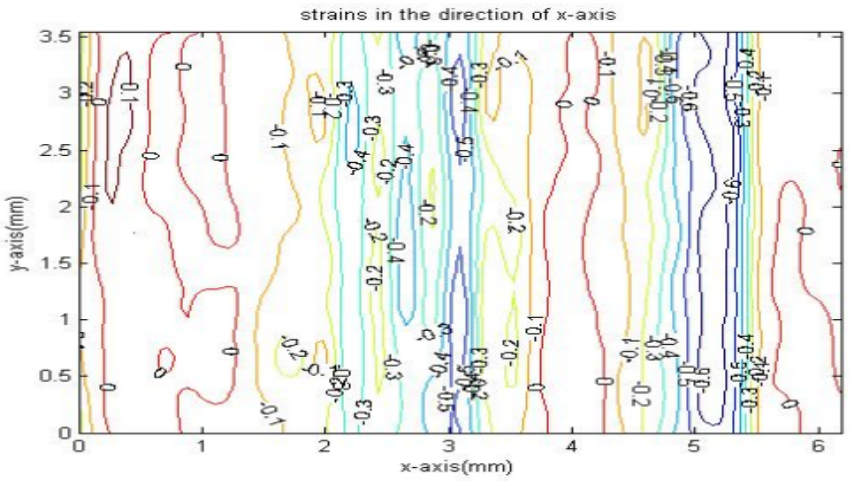

Figure 6.2 Final strain levels in the sample B-1-12-3

By looking at Figure 6.3 it can be seen that the strain in the second region is generated at the beginning of the compression. In the strains calculated from the middle of the compression, the strain in that region is close to final strain levels. Deformation in the first region has just started to take place. That region has slightly higher strain than the surrounding areas, but the strain level is still small. The rest of the deformation takes place mostly in the first region. The strain level in the first region rises during the latter part of the deformation.

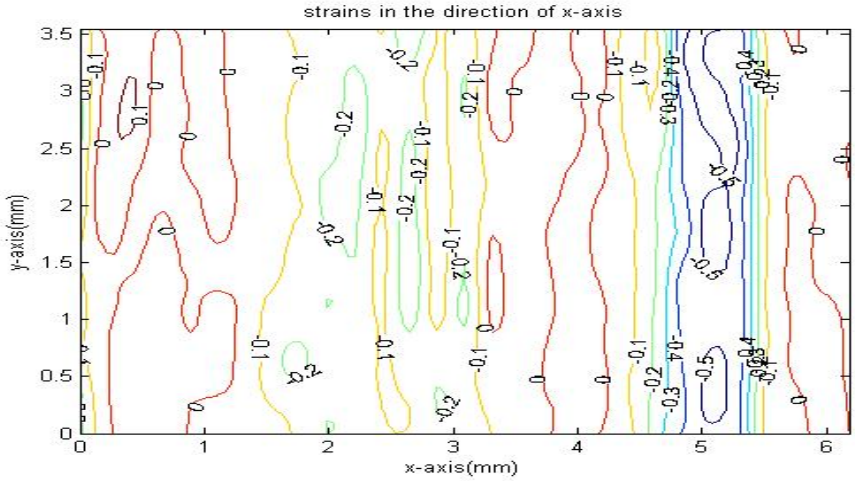

Figure 6.3 Strain levels in the middle of the compression of sample B-1-12-3

The deformation process as a function of the time can be seen in Figure 6.4. It shows the strain in the highest measured row of the sample as a function of time. The strain is given as an absolute value for easier viewing. The x-axis in the diagram shows the position in the sample along its x-axis. The y-axis shows the time and the z-axis is the absolute value of the strain. The diagram confirms that the deformation takes place initially in the right side of the sample and then on the other side.

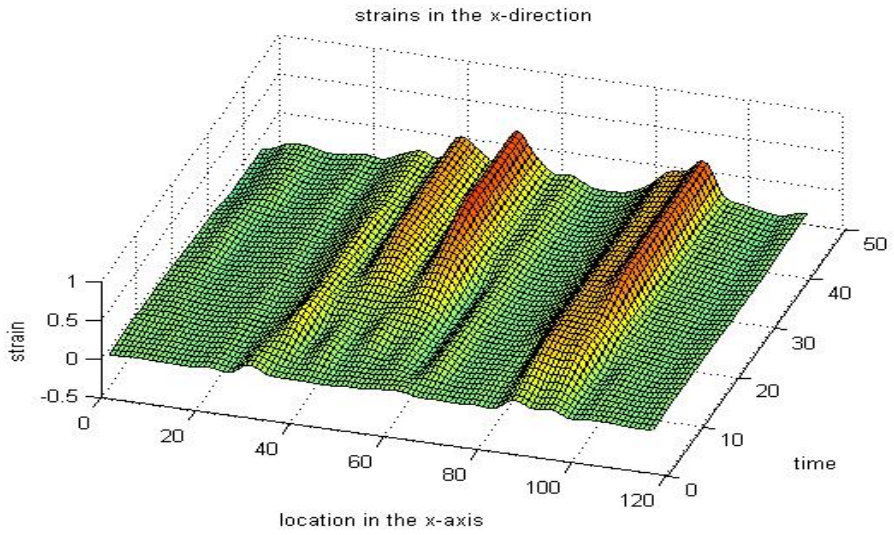

Figure 6.4 Strain in one row of the sample as a function of a time.

6.1.2 Sample A-1-20-5

Sample A-1-20-5 is shown in Figure 6.5. It has three latewood layers that are nearly perpendicular to the compression. The sample had medium level of fatigue. The compression was performed at 20 °C.

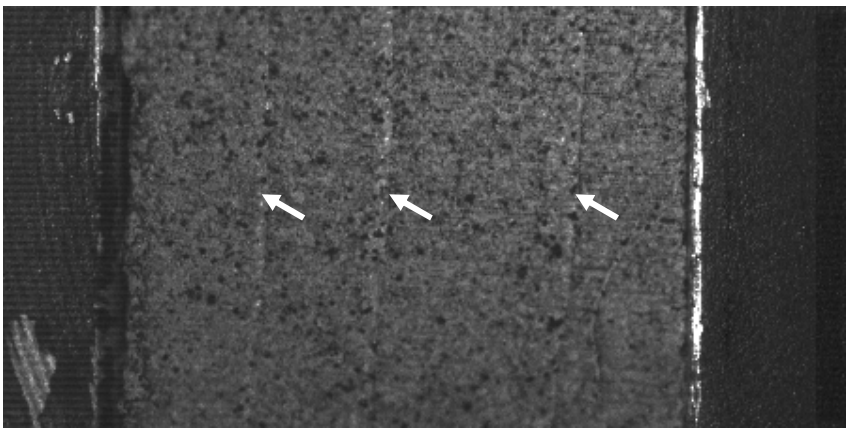

Figure 6.5 Growth rings of sample A-1-20-5

The strain distribution is shown at Figure 6.6.The highest strain region is at the right side of the sample. There are two other regions where the strain is clearly larger than in surroundings. In the region on the right, the strain is around -0.4 peaking at higher level than -0.5. In the two other regions the strain levels stay in the region of -0.3.

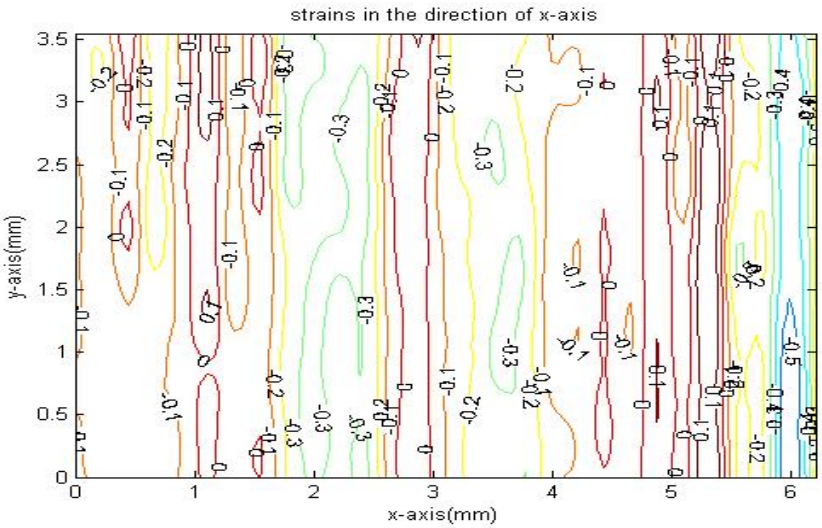

Figure 6.6 Final strain levels in sample A-1-20-5

The strain regions are concentrated in the earlywood layers of the growth rings. In the latewood regions strain levels are small. The strain levels from the middle of the compression are presented in Figure 6.7. It can be seen that in all the regions, the strain levels are lower than the final levels. The greatest difference in strain is on the right side of sample.

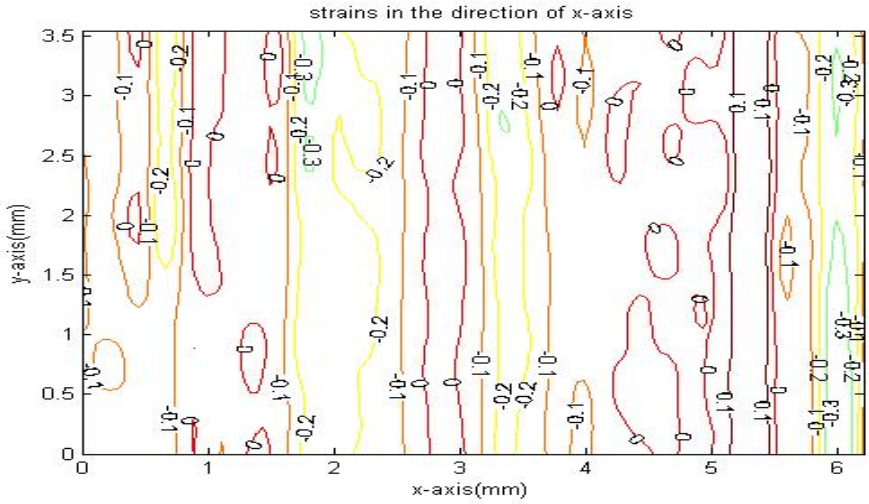

Figure 6.7 Strain levels in the middle of the compression of sample A-1-20-5

6.1.3 Sample B-1-4-3

Sample B-1-4-3 had three latewood layers. They were located slightly diagonally from down left to up right, which can be seen in Figure 6.8. The middle latewood layer is hard to see, but it is still just distinguishable. The sample had a high fatigue level and the compression was performed at 20 °C.

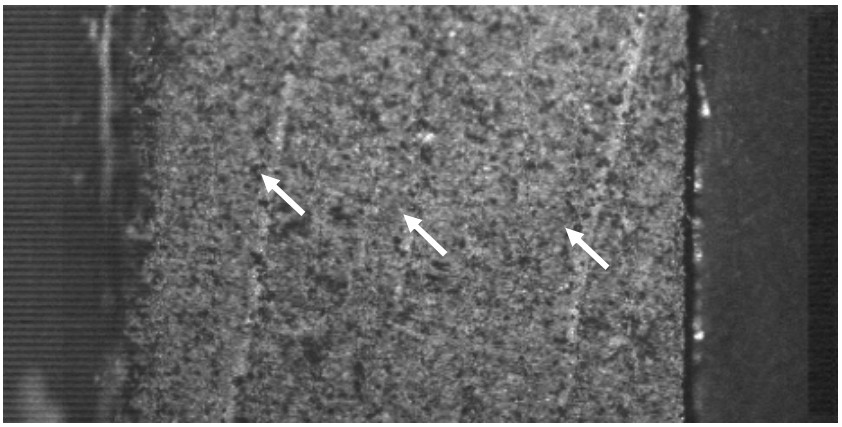

Figure 6.8 Growth rings of sample B-1-4-3

The strain levels are concentrated on four narrow regions as can be seen in Figure 6.9. The maximum strain levels in these regions are around -0.3 and strain above -0.4 are only attained at a few locations. The regions with highest strain are diagonal. They have the same orientation as the growth rings.

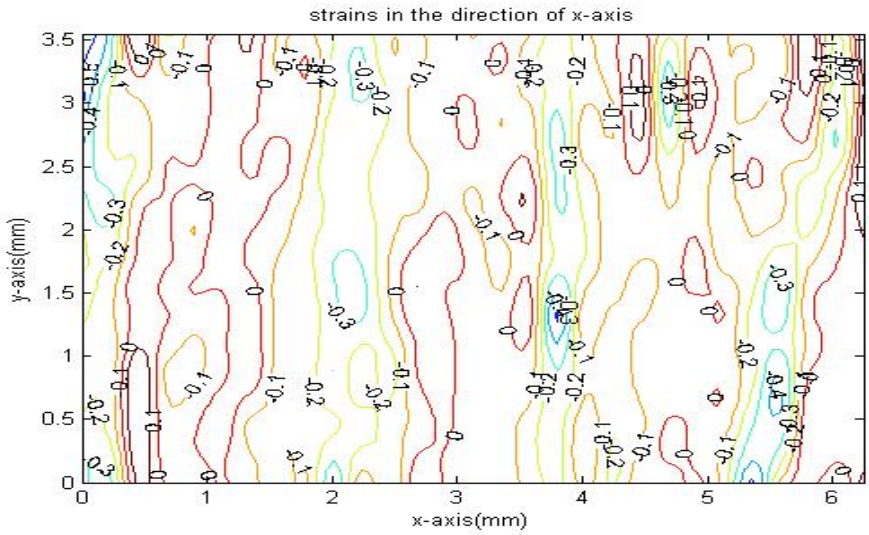

Figure 6.9 Final strain levels in sample B-1-4-3

At the beginning of the compression the strain is distributed quite evenly. Clear strain regions cannot be seen in Figure 6.10. The region which has the highest final strains has very little strain at this stage. During the rest of the compression the deformation will take place mainly in that region, while in the other regions strain increases nominally.

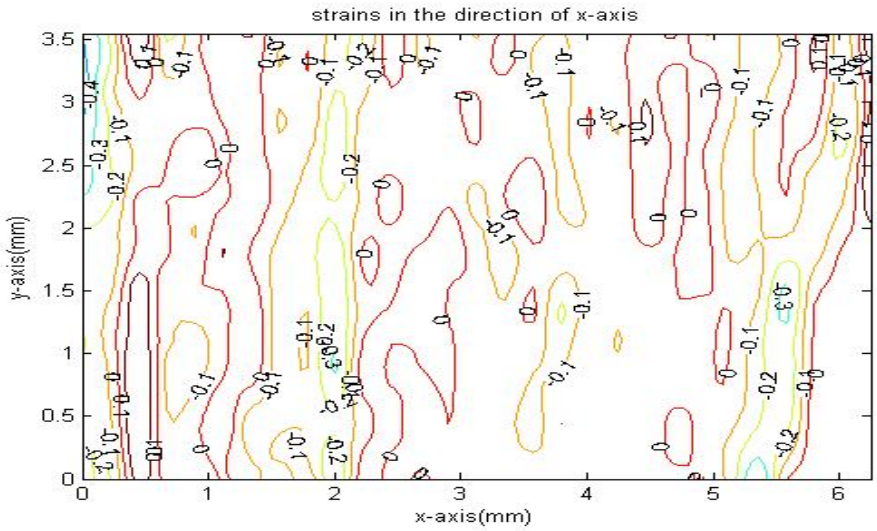

Figure 6.10 Strain levels in the middle of the compression of sample B-1-4-3

6.1.4 Sample B-5-5-4

Sample B-5-5-4 had two latewood layers and three earlywood layers in it. The late wood layers are marked in Figure 6.11 with white arrows. The right latewood layer is not easily distinguished. The sample had no fatigue added to it before testing. The compression was performed at 130 °C.

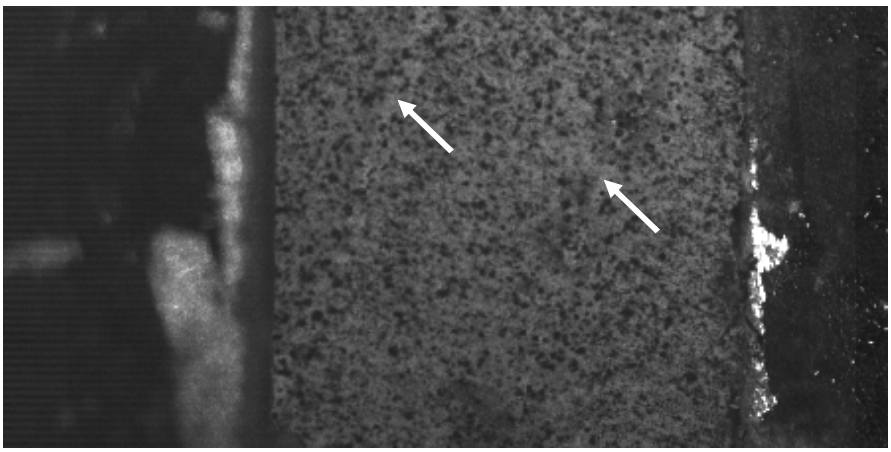

Figure 6.11 Growth rings of sample B-5-5-4

The strain levels were concentrated on the right side of the sample and in the earlywood layer between the latewood layers. It the earlywood on the right side of the sample the deformation was large (Figure 6.12). The strain levels in this area reached almost -1.0, which would mean complete deformation where the whole of the original length is lost. To attain such high strain levels in wood, very high stress is needed. The stress required increases rapidly when higher strain levels of more than -0.5 are attained. The high strain level measured is caused by inaccuracy of the algorithm in locations of high deformation. The deformation is large but the measured values are somewhat too large.

The strain region is slightly diagonal, which matches the orientation of the growth ring layers. The middle region of earlywood has strain levels from -0.2 to -0.4 so the strain levels are not very large, but the region itself is large.

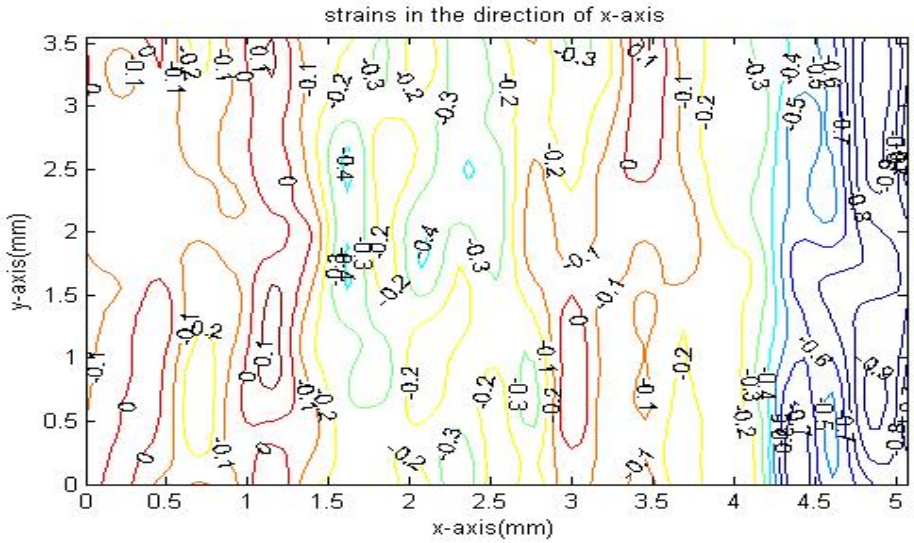

Figure 6.12 Final strain levels in sample B-5-5-4

The strain levels from the middle of the compression shows that the deformation takes place mostly in the right layer during the first half of the compression (Figure 6.13). However, the strain levels at this point do not yet match the final strain levels, so in the rest of the compression the strains in that region will increase. The middle region is at this point divided into two narrower regions with a small strip between them, but during the rest of the compression the deformation will have most effect in that strip.

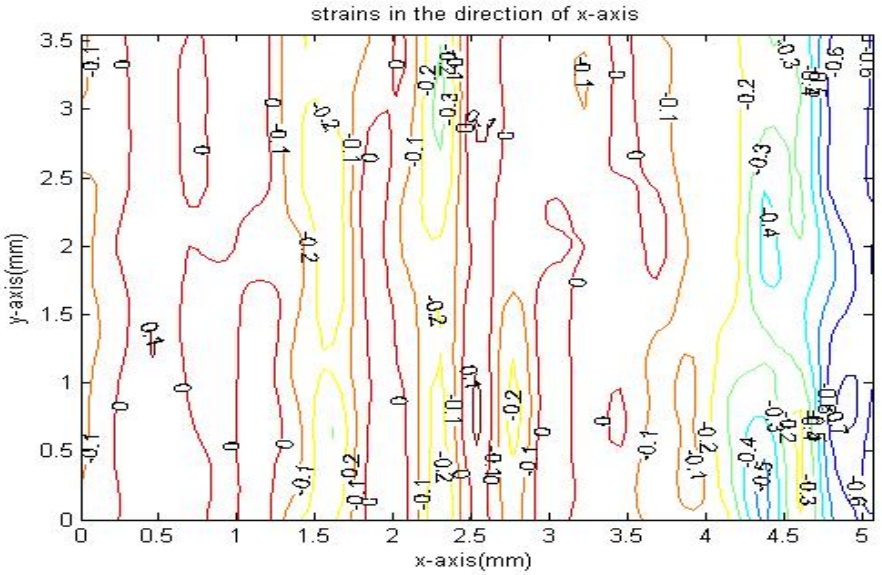

Figure 6.13 Strain levels in the middle of the compression of sample B-5-5-4

6.1.5 Sample A-1-10-5

Sample A-1-10-5 has three latewood layers and three earlywood layers. The latewood layers are marked in Figure 6.14 with white arrows. The sample had a low fatigue level and the compression was performed at 60 °C.

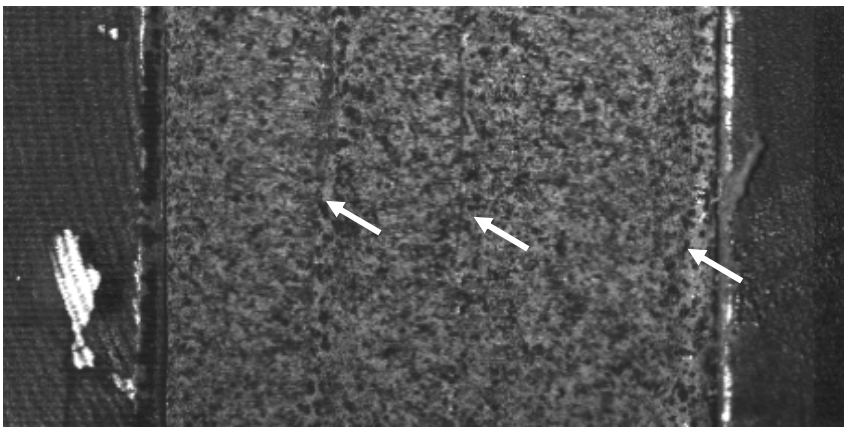

Figure 6.14 Growth rings of sample A-1-10-5

The strain is concentrated in two regions that are located on the right hand earlywood layers (Figure 6.15). In the far right region the magnitude of the strains is around -0.7 whereas in the other region the strain is only around -0.4.

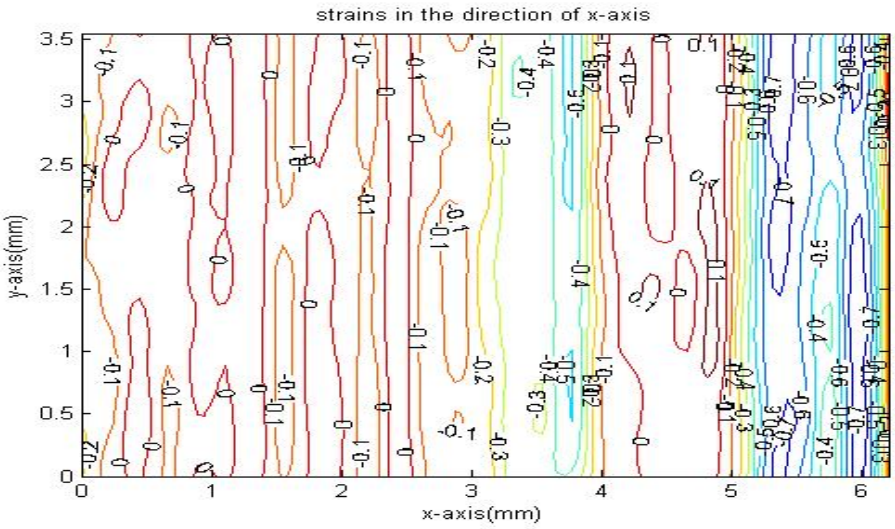

Figure 6.15 Final strain levels in sample A-1-10-5

At the beginning of the compression all the deformation is taking place at the right side of the sample (Figure 6.16). The strain level on that region is around -0.5 while in the middle part the deformation is just starting to happen.

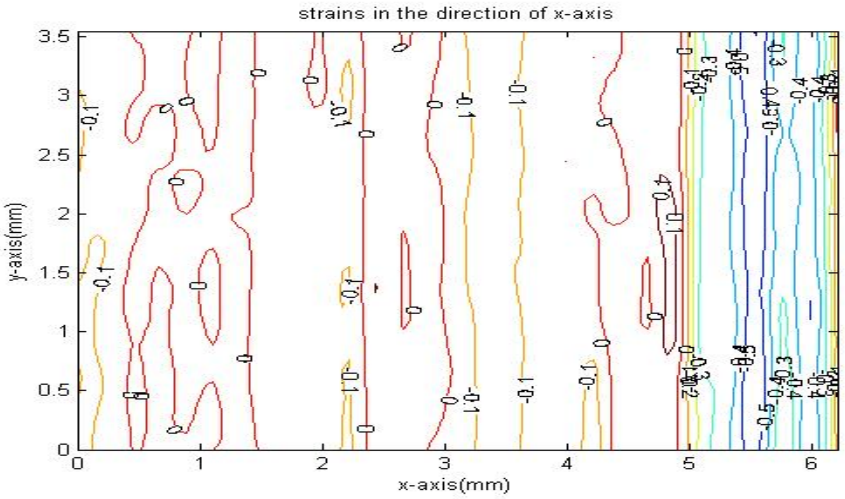

Figure 6.16 Strain levels in the middle of the compression of sample A-1-10-5

6.1.6 Sample A-1-3-2

Sample A-1-3-2 had three growth rings starting from the latewood at the left, ending in the very narrow earlywood layer at the right. The boiling during the heating process disturbed the painted surface and the growth rings cannot be detected in the sample. The sample is shown in Figure 6.17. The earlywood and latewood layers can be detected in the photographs taken of the samples before the painting. In this case the strain maps give a clear indication of the location of the different layers. The latewood layers of the sample were very thick, probably an indication of reaction wood. The sample had a low fatigue level and the compression was performed at 100 °C.

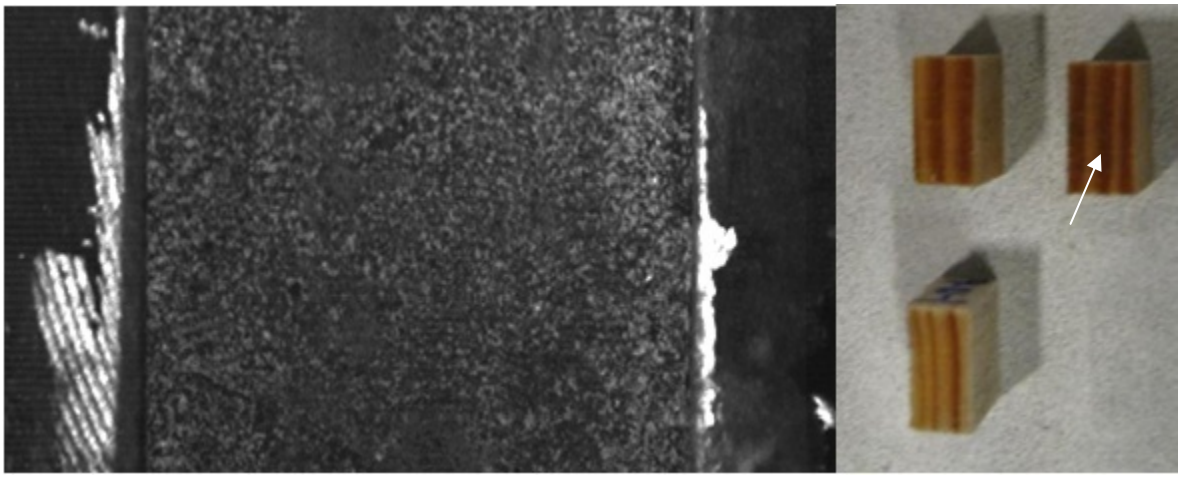

Figure 6.17 Sample A-1-3-2. The painting was destroyed so the location of the growth rings was checked from a photograph of the sample

The strain levels in each of the earlywood layers were extremely high as can be seen in Figure 6.18. In the middle layer a strain of -1.0 was attained. That high strain value was caused by the inaccuracy of the computation algorithm, although the deformation is still very large in that area. Furthermore, in the other strain regions very high strain levels are attained. The error may be partially caused by water that started coming out of the sample at the end of the deformation. This water prevents a view of the sample. Although the strain levels are large, the regions where the strain is located are very narrow, which corresponds to narrow earlywood layers.

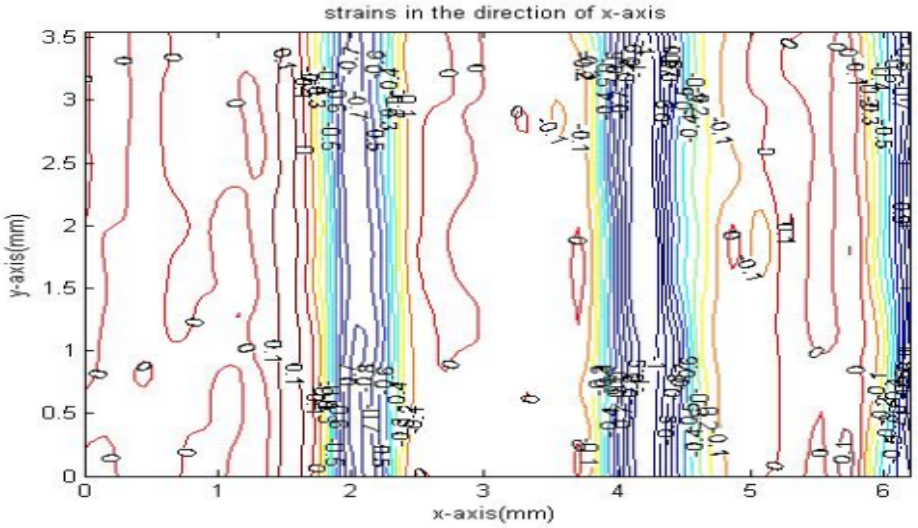

Figure 6.18 Final strain levels in sample A-1-3-2

The strain levels in the middle of the compression can be seen in Figure 6.19. In the first half of the compression, the deformation takes place in the middle earlywood layer. In other strain regions deformation is just starting to take place.

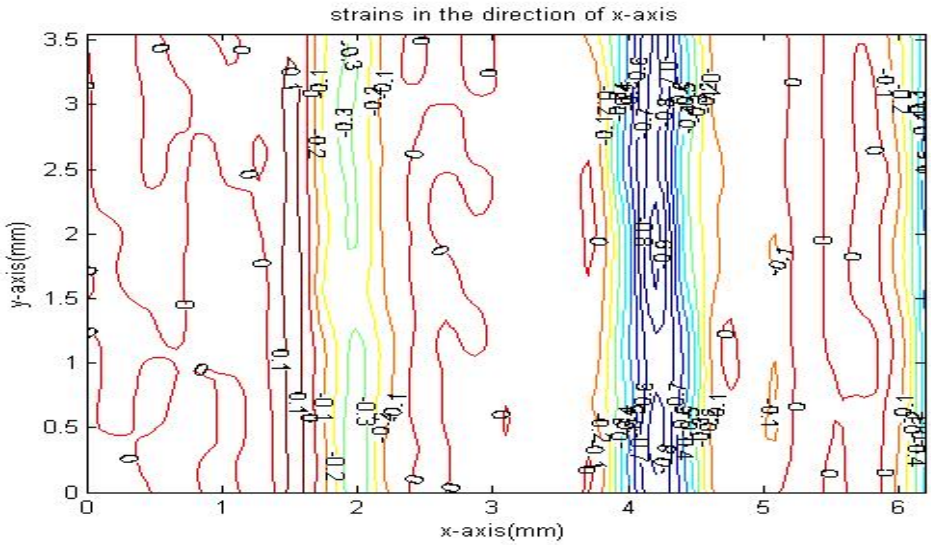

Figure 6.19 Strain levels in the middle of the compression of sample A-1-3-2

6.1.7 Sample A-1-11-5

Sample A-1-11-5 had three slightly diagonal growth rings. The latewood layers of the growth rings are shown in Figure 6.20. The sample had a medium fatigue level and the compression was performed at 130 °C.

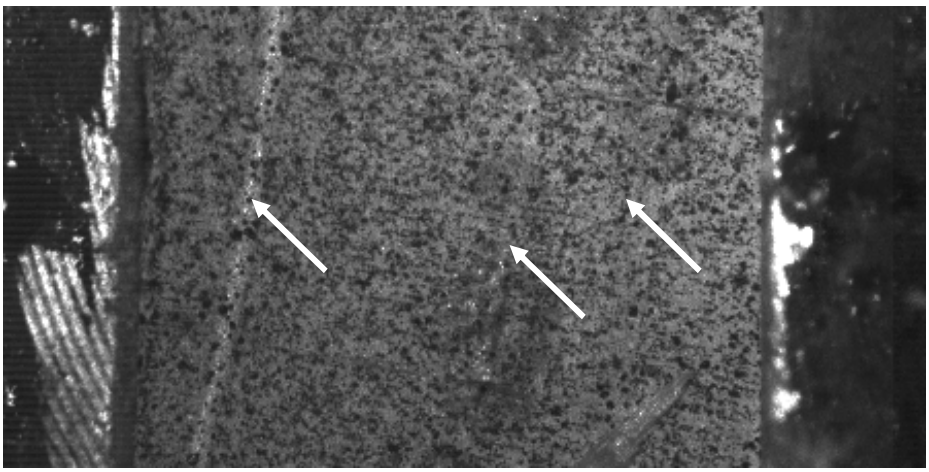

Figure 6.20 Growth rings of sample A-1-11-5

The strain was concentrated in the regions that match the earlywood layers. The regions are not as clear as in previous cases but there are no clear regions without strain. The highest strain was attained in the upper part of the sample around the 2 mm mark along the x-axis as shown in Figure 6.21. On the right side of the sample there is significant strain, but no clear region where the strains would be limited.

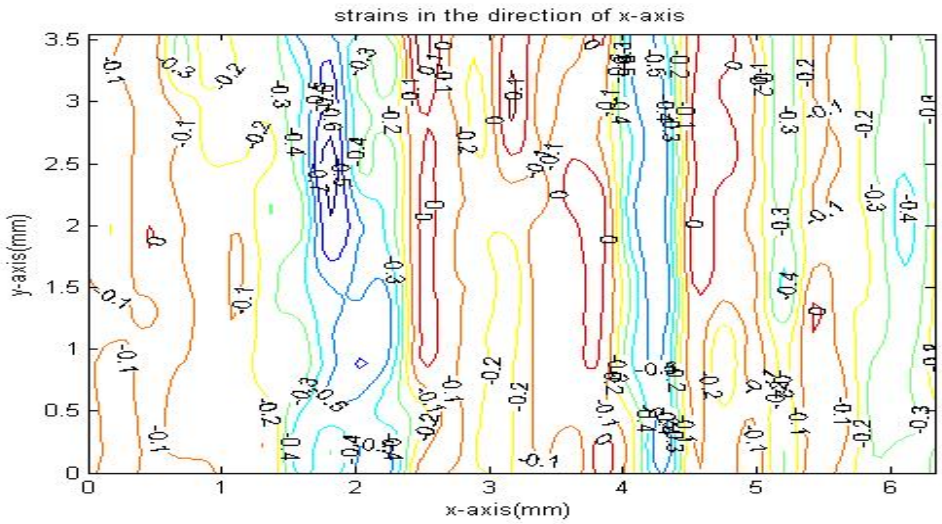

Figure 6.21 Final strain levels in sample A-1-11-5

Figure 6.22 shows the strain levels in the middle of the compression. It is seen that the strain is concentrated on the left side of the sample in the region which has the highest final strain levels. In the other part of the sample the strain is minimal but the regions where the strain will concentrate start to separate from their surroundings.

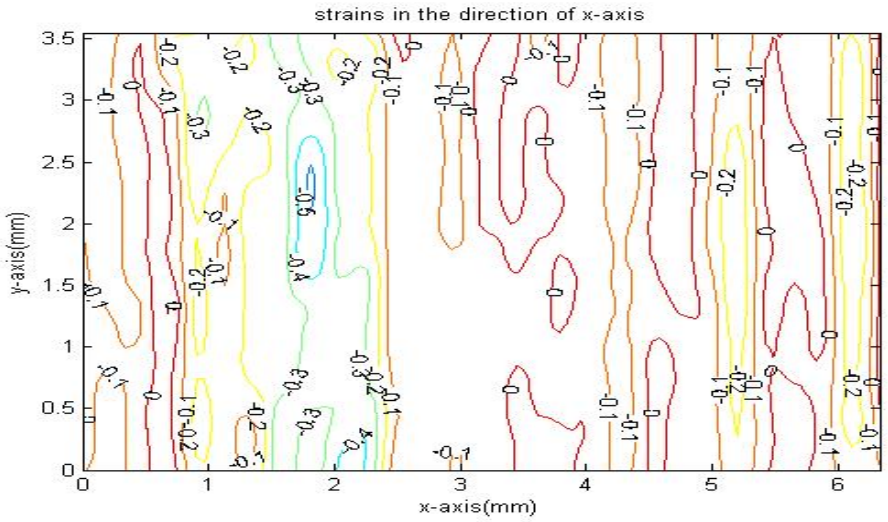

Figure 6.22 Strain levels in the middle of the compression of sample A-1-11-5

6.1.8 Sample A-1-12-2

The sample A-1-12-2 had three growth rings. The latewood layers of the sample were very thick. The latewood layers of the sample are marked in Figure 6.23. The middle layer is hard to distinguish because the paint surface was disturbed during the heating of the sample. The sample had a high fatigue level and the compression was performed at 130 °C.

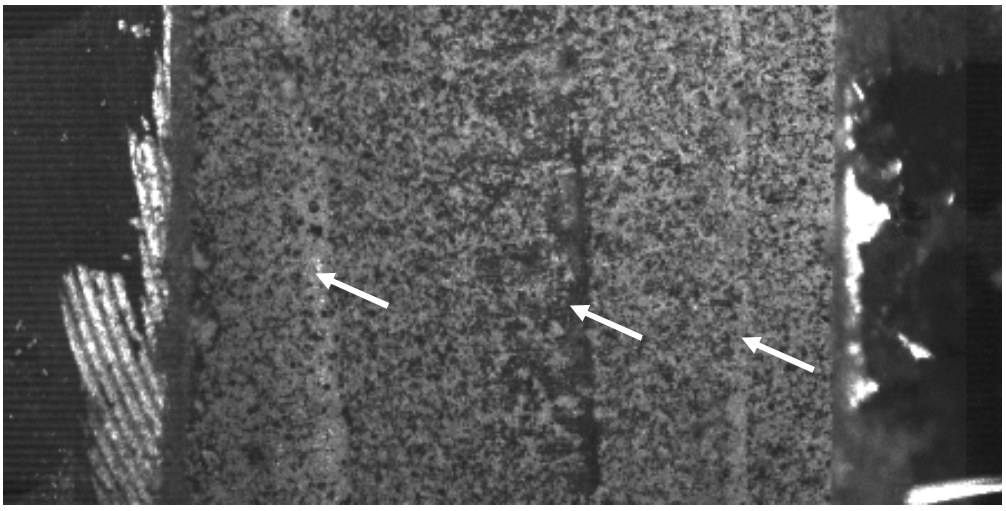

Figure 6.23 Growth rings of sample A-1-12-2

The strain levels can be seen in Figure 6.24. The strain is concentrated in three regions. All regions have a narrow high strain part where strain levels are more than -0.7. The region on the left has an additional large area with a lower strain of around -0.2. The strain regions again match the earlywood layers of the wood as the left hand layer was thicker than the other two layers.

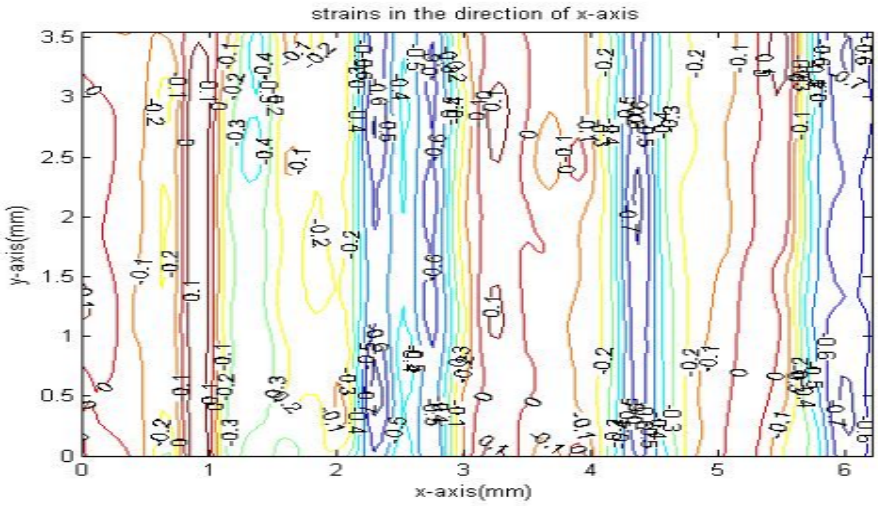

Figure 6.24 Final strain levels in sample A-1-12-2

The strain levels in the middle of the compression are shown in Figure 6.25. The deformation started in the left two regions and they have already almost attained the final deformation level. The rest of the compression will cause deformation in the right hand regio, which had, at that point, a strain level of around -0.2.

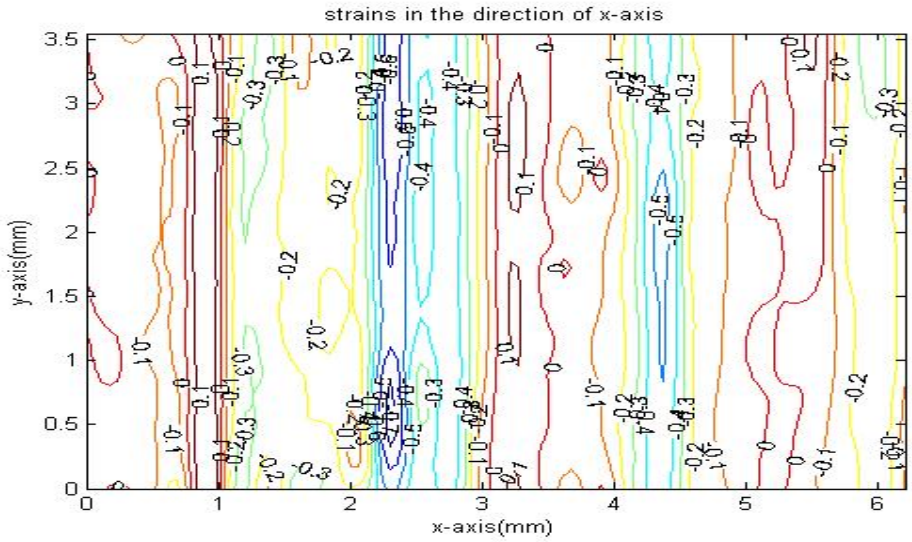

Figure 6.25 Strain levels in the middle of the compression of sample A-1-12-2

6.2 Local strain levels in earlywood and latewood

While the number of samples is not sufficient to draw statistically robust conclusions some initial conclusions can be derived from the results. In most of the samples analyzed it is clearly seen that the strain concentrates in the earlywood. Only a few samples had any strain in the latewood but all the samples had quite large strain levels in the earlywood. Strain in the earlywood was not distributed evenly and some earlywood layers had very little strain although most of them had high strain levels in the regions of -0.5.

The deformation in high strain areas does not happen evenly during compression. It was noted that at the beginning of the compression the deformation normally takes place in a different location from that found at the end of the compression. This is a logical consequence of the structure of the wood. The weakest cells deform first. Although the analysis algorithm computes the strain for small local areas, it still averages the strain over larger local areas.

Increasing the temperature and fatigue increased the magnitude of local strain levels. This trend was expected. The variation between the samples and the small number of test samples make it impossible to do a statistical analysis of the effects of temperature and fatigue. Differences in local strain levels between different high temperature tests were small. The same was true for strain levels in different fatigue levels. There is a clear rise in strain levels from samples with no fatigue to those which had been fatigued but differences between the different fatigue levels was not consistent.

7 Conclusions

The conclusions are divided into two parts. The first part concerns the measuring method. This consists of image acquisition and image analysis and how they worked in this application. The second part consists of conclusions from the analysis of the results. These conclusions consist of the analysis of the strain location and distribution in the wood samples. The effects of the fatigue and the temperature on local strain levels are also included.

The high-speed image acquisition and image analysis proved to be a useful tool for measuring strain levels in the wood samples. This kind of measurement system made it possible to define local strain levels, which is important with inhomogeneous materials. Image acquisition worked well and the quality of images proved to be sufficient for the analysis. With the development of camera technology it will be possible to acquire images with higher resolution at higher recording rate. That would lead directly to more accurate results. If the resolution of the images can be increased, the speckle size on the surface of the samples should be decreased so that maximum benefit can be obtained from the increased resolution. That, however, would mean that a new method is needed to create the surface pattern as spray painting cannot provide smaller droplets. One possibility would be to use a lens with such a high magnification that the deformation can be observed directly from the cell structure.

Local displacement vectors are defined by the cross-correlation function. The method worked well and with sufficient accuracy and generally there seemed to be no large errors or low correlation values. The accuracy of the displacements is limited by the resolution of the images and the size of the speckles in the surface pattern. At the locations where the deformations took place the correlation values were lower than elsewhere so the risk of error was higher at these locations. This problem could be adjusted if a good way to model local deformation could be found.

The distribution of the local strain levels in the wood gives useful information about the structure and the strength of the wood. In these measurements it was noted that the strain was concentrated on the softer earlywood layers and there was very little strain in the latewood layers. Raising the temperature or fatigue level did not have a clear effect on the distribution of the strain levels. Generally, increased temperature and fatigue levels increased the magnitude of the strain in the earlywood, while latewood still remained without strain. It was expected that in highly fatigued samples the latewood layers would have higher strain levels and the distribution would be more even. These results do not support that expectation but the number of samples analyzed is still too small to draw final conclusions.

In the measurements it was also noted that the strain is not distributed evenly in the earlywood. The softest parts of the earlywood are compressed first and as long as the load continues to be applied more earlywood cells are compressed. Because the softest part of the earlywood is normally grown at the beginning of the growth season, the buckling of the cells seemed to start at the beginning of the growth ring.

The temperature and the fatigue level clearly have an effect on the magnitude of the strain levels. This can be seen by comparing the room temperature test results with the other test results at the same fatigue level and by comparing the strain levels from the samples with no fatigue to the strain in the samples with fatigue but at the same temperature. Higher temperature and fatigue levels increase the strain levels in the sample. However, the differences in strain between the samples tested at different high temperatures are not large. Not enough samples were analysed to allow statistically reliable conclusions to be drawn. Greater differences had been expected but these results can be related to the properties of the wood. Because of the structure of wood, the samples were not identical and there were large variations between the samples. Even the number and the direction of the growth rings varied. This causes large variations in the results and a much larger amount of data is needed for reliable statistical analysis. The same applies to different fatigue levels.

Even though the effect of the environmental factors could not be accurately determined, this work provides valuable information on the structure of the wood. This information can be used when models of wood are designed. The wood models can be used in simulations to optimize different processes such as mechanical pulping with lower energy consumption. However, more tests will be needed to verify these results and to see whether other variables such as the direction of the loading have an effect on the strain levels.

References

1. Hertzberg, Richard W. “Deformation and fracture mechanics of engineering materials”, 4th ed. New York, Wiley, cop. 1996.
2. John B. Scalzi, "Stress and strain", in AccessScience@McGraw-Hill, http://www.accessscience.com, DOI 10.1036/1097-8542.660300
3. Norman E. Dowling, “Mechanical behavior of materials: engineering methods for deformation, fracture, and fatigue”, 2nd ed. Upper Saddle River (NJ), Prentice Hall, 1999.
4. Joel W. House, Peter P. Gillis, “Testing Machines and Strain Sensors” ASM Handbooks Online, vol8, Mechanical testing and evaluation, http://products.asminternational.org/hbk/index.jsp
5. John H. Zifcak, "Strain gage", in AccessScience@McGraw-Hill, http://www.accessscience.com, DOI 10.1036/1097-8542.658400
6. Wikipedia, http://en.wikipedia.org/wiki/Strain_gauge
7. Sutton, M.A., Wolters, W.J., Peters, W.H., Ranson, W.E. and McNeill, S.R., "Determination of Displacement Using an Improved Digital Correlation Method," Computer Vision, 1 (3), 133-139 (1983).
8. Chu, T.C., Ranson, W.E, Sutton, M.A. and Peters, W.H., "Applications of Digital-Image-Correlation Techniques to Experimental Mechanics," EXPERIMENTAL MECHANICS, 25, 232 -244 (1985).
9. Bruck, H.A., McNeill, S.R., Sutton, M.A. and Peters, W.H., "Digital Image Correlation Using Newton-Raphson Method of Partial Differential Correction," EXPERIMENTAL MECHANICS, 29, 261-267 (1989).
10. Chen, D.J. and Chiang, EP., “Computer Speckle Interferometry (CS1)”, Proceedings of the International Conference on Hologram Interferometry and Speckle MetroIogy, 49-58 (1990).
11. Chen, D.J. and Chiang, EP., "Optimal Sampling and Range of Measurement in Displacement-Only Laser-Speckle Correlation," EXPERIMENTAL MECHANICS, 32, 145-153 (1992).
12. Chert, D.J., Chiang, EP., Tan, Y.S. and Don, H.S., "Digital Speckle-Displacement Measurement Using a Complex Spectrum Method," Applied Optics, 32 (11), 1839-849 (1993).
13. Sjödahl, M. and Benehert, L.R., "Electronic Speckle Photography:Analysis of an Algorithm Giving the Displacement with Subpixel Accuracy," Applied Optics,32 (13), 2278-2284 (1993).

14. Sjödahl, M. and Benchert, L.R., "Systematic and Random Errors in Electronic Speckle Photography," Applied Optics, 33 (31), 7461-7471 (1994).

15. Sjödahl, M., "Electronic Speckle Photography: Increased Accuracy by Non-Integral Pixel Shifting," Applied Optics, 33 (28), 6667-6673 (1994).

16. Jame B. Wilson, "Wood properties", in AccessScience@McGraw-Hill, http://www.accessscience.com, DOI 10.1036/1097-8542.748600

17. Kettunen, Pentti O.,"Wood : structure and properties" Uetikon-Zuerich ; Enfeld (NH) : Trans Tech Publications, 2006. Materials science foundations, vol. 29-30

18. Wiedenhoeft,Alex C., Miller Regis B.,"Structure and Function of Wood" Handbook of wood chemistry and wood composites, ed Rowell, Roger M. USDA, Forest Service, Forest Products Laboratory, Madison, WI. 2005

19. Alén, Raimo,"Structure and chemical composition of wood" Forest products chemistry, Book 3 Papermaking science and technology, edt Stenius Per, Fapet OY, 2000

20. Schweingruber, Fritz, "Modification of the Xylem Within Plant" Atlas of Woody Plant Stems Evolution, Structure, and Environmental Modifications, Springer Berlin Heidelberg, 2006

21. Foulger, A.N. "Classroom Demonstrations of wood properties", U.S Department of Agriculture Forest Service, Forest Products Laboratory,1969

22. Uhmeir, Andreas, Salmén, Lennart, "Influence of Strain Rate and Temperature on the Radial Compression Behavior of Wet Spruce", Journal of Engineering Materials and Technology, 118 ,289–294 (1996).

23. Widehammar, Svante, "Stress-strain relationships for spruce wood: Influence of strain rate, moisture content and loading direction", Experimental Mechanics, 44, 44-48 (2006)

24. Kaiser, Michael Adam, "Advancements in the Split Hopkinson Bar Test" Master of Science thesis, Blacksburg, Virginia 1998, http://scholar.lib.vt.edu/theses/available/etd-41998-18465/unrestricted/ETD.pdf

25. Wikipedia, http://en.wikipedia.org/wiki/Hopkinson_bar

26. Blumenthal, William R., George T. (Rusty) Gray III, "Split-Hopkinson Pressure Bar Testing of Soft Materials" ,ASM Handbooks Online, vol8, Mechanical testing and evaluation, http://products.asminternational.org/hbk/index.jsp, 2003

27. Widehammar, S "A method for dispersive split Hopkinson pressure bar analysis applied to high strain rate testing of spruce wood" Doctoral thesis, Uppsala University, Division of Solid Mechanics, Sweden, 2007.

28. Photron Fastcam product sheet, http://www.photron.com/pdf/Fastcam_SA1_Datasheet.pdf

29. Litwiller, Dave “CMOS vs. CCD: Maturing Technologies, Maturing Markets” Photonics Spectra, August 2005

30. Pope, Robin M., Fry, Edward S. “Absorption spectrum (380–700 nm) of pure water. II. Integrating cavity measurements” Applied Optics vol. 36. p8710-8723 1997

31. Lu H., Cary, P. D.” Deformation Measurements by Digital Image Correlation: Implementation of a Second-order Displacement Gradient“EXPERIMENTAL MECHANICS, 40, 393-400 (2000).

Appendix 1: Labels of the samples

Sample name	File name	Test date	Test time	Temperature [C]
B-1-4-7 : 20k	011	2.12.	14:50	20,0
B-1-4-3 : 20k	010	2.12.	14:44	20,0
B-1-12-6 : 0k	013	2.12.	15:10	20,0
B-1-12-3 : 0k	012	2.12.	14:59	20,0
B-1-11-5 : 6k	014	2.12.	15:55	20,0
B-1-11-7 : 6k	017	2.12.	16:12	20,0
A-1-20-2 : 12k	016	2.12.	16:07	20,0
A-1-20-5 : 12k	015	2.12.	16:01	20,0
A-1-24-6 : 0k	009	2.12.	14:37	20,0
Sample name	**File name**	**Test date**	**Test time**	**Temperature [C]**
A-1-24-5 : 0k	019	3.12.	10:22	68,0
A-1-10-5 : 6k	020	3.12.	10:33	64,0
B-1-18-5 : 12k	021	3.12.	10:41	62,0
A-1-16-1 : 20k	022	3.12.	10:52	62,0
A-1-16-2 : 20k	018	3.12.	10:09	68,0
Sample name	**File name**	**Test date**	**Test time**	**Temperature [C]**
A-1-1-1 : 6k	023	3.12.	13:29	100,0
A-1-1-7 : 6k	027	3.12.	14:39	100,0
A-1-9-2 : 0k	024	3.12.	13:58	100,0
A-1-9-7 : 0k	028	3.12.	14:51	100,0
A-1-14-4 : 12k	025	3.12.	14:12	100,0
A-1-14-7 : 12k	029	3.12.	15:01	100,0
A-1-15-3 : 20k	026	3.12.	14:25	100,0
A-1-15-6 : 20k	030	3.12.	15:13	100,0
Sample name	**File name**	**Test date**	**Test time**	**Temperature [C]**
A-1-2-4 : 6k	039	3.12.	18:11	100,0
A-1-2-6 : 6k	034	3.12.	17:22	100,0
A-1-4-1 : 12k	031	3.12.	16:43	100,0
A-1-4-5 : 12k	035	3.12.	17:35	100,0
A-1-8-2 : 0k	032	3.12.	16:58	100,0
A-1-8-5 : 0k	036	3.12.	17:50	100,0
A-1-17-3 : 20k	033	3.12.	17:09	100,0
A-1-17-6 : 20k	038	3.12.	18:02	100,0

Sample name	File name	Test date	Test time	Temperature [C]
A-1-18-6 : 0k	042	4.12.	11:10	100,0
A-1-3-1 : 6k	039	4.12.	10:33	100,0
A-1-3-2 : 6k	043	4.12.	11:24	100,0
A-1-5-1 : 12k	040	4.12.	10:45	100,0
A-1-5-6 : 12k	044	4.12.	11:34	100,0
A-1-7-4 : 20k	041	4.12.	10:55	100,0
A-1-7-7 : 20k	045	4.12.	11:45	100,0
Sample name	**File name**	**Test date**	**Test time**	**Temperature [C]**
Test	046	4.12.	13:38	
B-5-5-1 : 0k	047	4.12.	13:45	134,6
B-5-5-4 : 0k	053	5.12.	14:10	130,0
B-1-17-6 : 6k	048	4.12.	13:55	129,6
B-1-17-7 : 6k	054	5.12.	14:21	130,0
A-1-11-1 : 12k	049	4.12.	14:11	130,0
A-1-11-5 : 12k	055	5.12.	14:35	130,0
A-1-12-2 : 20k	052	5.12.	1354	130,0

Appendix 2: Sample code

```
% Matlab script for analyzing strains in image series
% code by Valtteri Saari
% Program goes through all the bitmap images in
% the current folder.
% The strains are computed using correlations
% The locations of the control points at each frame
% are saved at gridxloc and gridyloc. The final strain values
% are saved in xstraintot
%%%%%%%%%%%%%%%%%%%%%%%%

% the sizes of correlation windows and
% the distance between different windows
W=15;
W2=7;
grid=10;

% First image is read and plotted
contents = dir('*.bmp');
filename1 = contents(1).name;
B1=imread(filename1,'bmp');
B1=double(B1);
B1=medfilt2(B1,[3 3]);
figure
imshow(B1,[10 130]);

% The area of interest is defined from the first image
[AoI(1),AoI(3)]=ginput(1);
hold on
plot(AoI(1),AoI(3),'+g')
[AoI(2),AoI(4)]=ginput(1);
plot(AoI(2),AoI(4),'+g')
xgrid=AoI(1):grid:AoI(2);
ygrid=AoI(3):grid:AoI(4);
[gridyloc gridxloc]=ndgrid(ygrid,xgrid);
xmove=zeros(length(ygrid),length(xgrid));
ymove=zeros(length(ygrid),length(xgrid));
xoffset1=zeros(length(ygrid),length(xgrid));
yoffset1=zeros(length(ygrid),length(xgrid));
xoffset2=zeros(length(ygrid),length(xgrid));
yoffset2=zeros(length(ygrid),length(xgrid));
corrs=zeros(length(ygrid),length(xgrid));
%%%%%%%%%%%%%%%%%%%%%%%%
% plots the first image and original grid
 figure
imshow(B1,[10 130]);
 hold on
plot(gridxloc(:,:),gridyloc(:,:),'y.');
hold on
```

```
%%%%%%%%%%%%%%%%%%%%
%  The main loop

for k = 1:numel(contents)-1

   % Next image is read from the folder
  filename2 = contents(k+1).name;
  B2=imread(filename2,'bmp');
  B2=double(B2);
  B2=medfilt2(B2,[3 3]);

%%% The movement of each grid point between consecutive
%%% frames is computed in loop
  for i=1:length(ygrid)
    for j=1:length(xgrid)
        % First interrogation areas around the point is
        % taken from the both frames
        locy=gridyloc(i,j);
        locx=gridxloc(i,j);
        tempy=locy-W:1:locy+W;
        tempx=locx-W:1:locx+W;
        [ytemp xtemp]=ndgrid(tempy,tempx);
        template=interp2(B1,xtemp,ytemp);
        temp2y=locy-W-1:1:locy+W+1;
        temp2x=locx-W-1:1:locx+2*W;
        [y2temp x2temp]=ndgrid(temp2y,temp2x);
        A=interp2(B2,x2temp,y2temp);

        % Areas are correlated and location of the peak is defined
        % and initial displacement is defined
        CC=normxcorr2(template,A);
         [~, imax] = max(abs(CC(:)));
         [ypeak, xpeak] = ind2sub(size(CC),imax(1));
         corr_offset = [(xpeak-size(template,2)); (ypeak-
size(template,1))];
             rect_offset= [1 ;1];
            offset = corr_offset-rect_offset;
        xoffset = offset(1);
        yoffset = offset(2);

        xoffset1(i,j)=xoffset;
        yoffset1(i,j)=yoffset;
        locx2=locx+xoffset1(i,j);
        locy2=locy+yoffset1(i,j);

        % Second interrogation areas are taken using
        % the estimate of the initial displacement
        tempy=locy-W2-0.5:1:locy+W2+0.5;
        tempx=locx-W2-0.5:1:locx+W2+0.5;
        [ytemp xtemp]=ndgrid(tempy,tempx);
        template2=interp2(B1,xtemp,ytemp,'cubic');

        temp2y=locy2-W2-1.5:1:locy2+W2+1.5;
        temp2x=locx2-W2-1.5:1:locx2+W2+1.5;
        [y2temp x2temp]=ndgrid(temp2y,temp2x);
        A2=interp2(B2,x2temp,y2temp,'cubic');
```

```
        CC2=normxcorr2(template2,A2);
        [max_c, imax] = max(abs(CC2(:)));
        corrs(i,j)=max_c;

        [ypeak, xpeak] = ind2sub(size(CC2),imax(1));
         corr_offset = [(xpeak-size(template2,2)); (ypeak-
size(template2,1))];
              rect_offset= [1 ;1];
             offset = corr_offset-rect_offset;
        xoffset = offset(1);
        yoffset = offset(2);

        % New displacement is computed in sub pixel accuracy
        [y1,x1]=ndgrid(1:3);
        [Y1,X1]=ndgrid(1:0.1:3);
        CC3=interp2(x1,y1,double(CC2(ypeak-1:ypeak+1,xpeak-
1:xpeak+1)),Y1,X1,'cubic');
        [max_c, imax2] = max(abs(CC3(:)));
        [ypeak2, xpeak2] = ind2sub(size(CC3),imax2(1));
        ymove2=(ypeak2-11)/10;
        xmove2=(xpeak2-11)/10;

        xoffset2(i,j)=xoffset+xmove2;
        yoffset2(i,j)=yoffset+ymove2;

    end
  end
  % Computed displacements are combined to
  % total displacements between frames in two
  % directions
  xmove=xoffset1+xoffset2;
  ymove=yoffset1+yoffset2;

%%%%%%%%%%%%%%%%%%%%%%%%%%%%%%%%%%%%%%%%%%%%%%%%%%%%
% Post processing of the displacement vectors
%%%%%%%%%%%%%%%

  xlimit=1.5;
  ylimit=0.7;
    xmovemed=median(xmove);
  ymovemed=median(ymove);
    for i=1:size(xmove,1)
      for j=1:size(xmove,2)
            if (abs(xmove(i,j)-xmovemed(j))>xlimit || abs(ymove(i,j)-
ymovemed(j))>ylimit)
                xmove(i,j)=xmovemed(j);
                ymove(i,j)=ymovemed(j);

            end
      end
    end
xmove=medfilt2(xmove,[3 1]);
ymove=medfilt2(ymove,[3 1]);
```

```
%%%%%%%%%%%%%%%%%%%%%%%%%%%%%%%%
% New locations for control points are computed
gridxloc(:,:,k+1)=gridxloc(:,:,k)+xmove;
gridyloc(:,:,k+1)=gridyloc(:,:,k)+ymove;
%%%%%%%%%%%%%%%%%%%%%%%%%%%%%%%%
% Local strains between original and current frame are computed

xstraintot=zeros(length(ygrid)-1,length(xgrid)-1);
  for i=1:length(ygrid)-1
    for j=1:length(xgrid)-1

xstraintot(i,j)=(((gridxloc(i,j+1,k+1)+gridxloc(i+1,j+1,k+1))/2-
(gridxloc(i,j,k+1)+gridxloc(i+1,j,k+1))/2)-grid)/(grid);
    end
  end

%%%%%%%%%%%%%%%%%%%%%%%%%%%%%%%%
% plot of control points

figure
imshow(B2,[10 130]);
hold on
plot(gridxloc(:,:,k+1),gridyloc(:,:,k+1),'y.');
hold on

% The current frame is replaced by next
% before the new frame is read
  B1=B2;
  end
```